博士論文

論文題目　Analysis of mechanisms for stem-like properties induced by growth factors in breast cancer

（乳癌における増殖因子刺激によるがん幹細胞性維持機構の解析）

氏　　名　　富永　香菜

Analysis of mechanisms for stem-like properties induced by growth factors in breast cancer

（乳癌における増殖因子刺激によるがん幹細胞性維持機構の解析）

Internal Medicine
内科学専攻

Supervisor; Prof. Arinobu Tojo
指導教員;　東條 有伸

Applicant; Kana Tominaga
申請者氏名;　富永 香菜

Table of contents

1. Abstract

Breast cancer stem cells (BCSCs) are thought to give rise to breast cancer; however, there is currently no appropriate therapy targeting BCSCs. BCSCs are thought to be maintained in cancerous tissues by increased frequency of symmetric cell division at the expense of asymmetric cell division, although how this occurs remains largely unknown. In the present study, I discovered that the interaction between the Semaphorin (Sema)- molecules interacting with CasL 3 (MICAL3) signaling is a key pathway in the symmetric division of cancer stem-like cells. Knockdown of *MICAL3* inhibited tumor sphere formation and tumor initiating activity—properties of cancer stem-like cells—in patient-derived primary breast cancer cells and in a patient-derived xenograft (PDX) model. Stimulation with Sema3A or 3B—ligands that activate the monooxygenase domain of MICAL3—induced tumor sphere formation; complex formation involving MICAL3, CRMP2, and Numb (a key regulator of symmetric-asymmetric division); and stabilization of Numb in breast cancer cells. Overexpression of wild-type MICAL3, but not a version with a mutated monooxygenase domain, increased tumor sphere formation. Moreover, Neuropillin-1 (NP1), a receptor for Sema3, was specifically expressed at high levels in a BCSC-enriched population, and NP1-positive cells induced tumor sphere formation. Finally, I showed that knockdown of *MICAL3* reduced symmetric division but increased asymmetric division in NP1-positive cancer stem-like cells that express high levels of Numb. Thus, the

Sema3/MICAL3/CRMP2/Numb pathway appears to play a critical role in the symmetric division of cancer stem-like cells to expand the pool of BCSCs, and the process is mediated by the monooxygenase activity of MICAL3. I therefore provide a rationale for eradicating BCSCs by blocking the symmetric division of cancer stem-like cells by targeting molecules in this pathway.

2. Abbreviation

BCSCs; breast cancer stem cells

CRMP2; collapsin response mediator protein 2

EGF; epidermal growth factor

FAD; flavin adenine dinucleotide

FGF; fibroblast growth factor

HRG; heregulin

IGF2; insulin-like growth factor 2

MICAL3; molecules interacting with CasL 3

NAb; neutralizing antibody

NP; neuropilin

PDX; patient-derived xenograft

PLA; proximity ligation assay

ROS; reactive oxygen species

SCM; sphere culture medium

Sema; semaphorin

3. Introduction

Breast cancer is the most common type of cancer among women not only in Japan but also throughout the world. The incidence of breast cancer and the number of deaths resulting from the disease have increased among Japanese women in recent years, and are estimated to further increase in the future, partly due to the prevalence of a westernized life style, and an aging population.

Subtypes of breast cancer are classified clinically based on immunohistochemical staining patterns of the tumor tissue as follows: luminal A, luminal B, HER2-positive, and triple negative. The luminal A and luminal B subtypes are positive for hormone receptors, estrogen or progesterone receptors, and the luminal B subtype shows a higher Ki67 index, meaning a higher proliferative capacity, than the luminal A subtype[1]. The triple negative subtype stains negative for the hormone receptors and for HER2. Recent advances in medical technology have led to the development of molecular targeted therapy for breast cancer patients with tumors that express the hormone receptors or HER2[2,3]. In addition to endocrine therapy, molecular therapies targeted against the receptor tyrosine kinase HER2/ErbB2 are commonly used to treat breast cancer patients in the clinic, in cases HER2 is overexpressed in the cancer tissues, referred to as HER2-positive cases[4,5]. Conventional chemotherapy is used to treat the triple negative subtype. Although a significant number of patients have responded well to this

approach, they may still experience metastasis or recurrence, even after complete tumor resection and/or systemic treatment involving chemotherapy and/or radiotherapy. In particular, some patients with tumors of the luminal B or triple negative subtype have shown a high incidence of metastasis or recurrence. Tumor recurrence or metastasis may occur even after a long latent period, which, in the case of breast cancer, can often be more than 10 years[6]. When recurrence or metastasis occurs, patients show poor prognosis, because of a resistance to anticancer drugs.

It was previously believed that tumors were comprised of a homogeneous population of cancer cells, where mutations in the genome lead to abnormal cell proliferation, preventing cell death. However, recent evidence indicates that tumors are in fact comprised of heterogeneous cell types[7,8]. It is thought that these heterogeneous tumor tissues are maintained in a hierarchical organization involving a relatively small number of cancer stem cells and higher numbers of dividing progenitor cells and differentiated tumor cells (Figure 1). Cancer stem cells are thought to survive in their surrounding microenvironment, the so-called cancer stem niche[9,10]. These niche cells include tumor cells, which are the progeny of the cancer stem cells. It is thought that cancer stem cells may survive after systemic treatment by using the niche cells to protect them from this stressful environment. Moreover, recent evidence suggests that cancer cells themselves display plasticity, in that they can acquire

cancer stem cell properties[11,12]. Hence, cancer stem cells are not easy to eliminate, and may lead to metastasis and recurrence. Although it is likely that there are general mechanisms by which the cancer stem cell-state is stabilized in the cancer stem cell niche, these molecular mechanisms are largely unknown, and therefore there is still no targeted therapy against cancer stem cells that can be clinically implemented. Thus, there is an urgent need to identify molecules that play an important role in stabilization of the stem cell state, which would provide a rationale for developing novel molecular targeted therapies against cancer stem cells.

Breast cancer stem cells (BCSC) were first reported in 2003[13], when Al-Hajj et al., suggested their existence using patient-derived breast cancer cells. They showed enrichment of BCSC in a $CD44^{high}CD24^{low}$ cell population sorted by flow cytometry, and that this cell population had a high tumor-initiating activity when inoculated into the mammary fat pads of immunodeficient mice. Subsequently, it has been reported that epithelial cell adhesion molecule (EpCAM), CD10, β1 integrin (CD29), α6 integrin (CD49f), and CD133 may be used as cell surface markers of BCSCs[14–18]. It also has been reported that the Notch, Wnt, Hippo and mTOR signaling pathways are involved in the self-renewing activity of BCSC and in the tumorigenicity of breast cancer cells[19–22].

The in vitro tumor sphere formation assay has been established as an assay for BCSC [23](Figure 2). Tumor spheres are floating cell aggregates that include cancer stem-like cells. These spheres are obtained by culturing cancer cells in a defined sphere culture medium (SCM) that contains a cocktail of growth factors, including epidermal growth factor (EGF), basic fibroblast growth factor (bFGF) and hormones. In breast cancer tissues, cancer cells derived from epidermal tissues maintain contact with adjacent cells, resulting in the formation of solid tumors. These tumor cells stimulate each other via adherent signals for their survival. Normally, when these cells are trypsinized in vitro, the resulting single cells lose these adherent signals, stop dividing and some will eventually undergo apoptosis. This phenomenon is termed ‘anoikis’[24]. However, it is thought that cancer cells with stem-like properties are resistant to anoikis and are therefore able to divide in suspension. When these cells are sufficiently diluted and cultured under floating conditions, they are able to divide, giving rise to cell aggregates or spheres. Thus, a tumor sphere assay using patient-derived primary cancer cells at early passages may facilitate the enrichment of cancer cells with stem-like properties from the original the cancer tissue source. It is important to analyze primary cancer cells because although cancer cell lines may have gained some properties of cancer stem cells, when they are immortalized, they often lose the characteristics of the cancer tissues from which they originated. It is technically difficult to culture primary breast cancer cells freshly obtained from patients; however, I have established the necessary techniques.

By using patient-derived primary breast cancer cells, The laboratory which I belong to previously showed, using patient-derived primary breast cancer cells, that a single growth factor, heregulin (HRG), a ligand of HER3/ErbB3, was able to stimulate sphere formation in a $CD44^{high}CD24^{low}$ cell population that is thought to be enriched for breast cancer stem cells, but not in a control $CD24^{high}$ cell population, via activation of the HER2/3-PI3K/NFκB pathway[23] (Figure 3A and B). Given that the HER2/3-PI3K/NFκB pathway contributes to the maintenance of cancer stem cells in breast cancer tissues, I employed a method to systematically analyze the gene expression profiles over time in breast cancer cells upon stimulation with HRG, in order to identify specific pathways that play a critical role in these cancer stem cells and their niche (Figure 4A, B). This method uncovered a number of candidate downstream molecules, many of which may play a role in the interaction between cancer stem cells and their niche. Among these, I discovered that insulin-like growth factor 2 (IGF2) is produced by niche cancer cells and by cancer cells with stem-like properties. IGF2 binds to IGF-1R, which is specifically expressed in cancer cells with stem-like properties, and activates the PI3K pathway, leading to expression of the ID1 transcriptional regulator, which is required to maintain stemness (Figure 5, Tominaga et al., under reviewed).

Semaphorin The Semaphorin (Sema) family of membrane-bound or secreted proteins comprises 20 members in vertebrates[25]. It was initially reported that Sema relays repulsive

signals for axon guidance during development of the neural network[26–28] (Figure 6). Subsequently, it was reported that Semas are also secreted from immune cells, vascular endothelial cells and several types of cancer cells, and play important roles by acting in an autocrine or paracrine manner[29,30]. Neuropilin (NP) and plexin form a receptor complex for Semas[31]. NP serves as the primary receptor for ligand binding, whereas the plexin coreceptor transduces the Sema signal via the intracellular domain. Type 3 Semas contain seven members (Sema 3A~G) in vertebrates[32]. The function of type 3 Semas remains controversial in cancer, because it has been reported that type 3 Semas can act as both tumor suppressors and activators in a context-dependent manner[30,33,34]. It was recently reported that some type 3 Semas promote tumorigenesis, anti-apoptosis and metastasis[35,36]. In particular, Sema 3C promotes tumor survival by activating the Rac1-NFκB axis via the PlexnA/NP1 receptor complex in glioma stem cells[37].

Genes encoding molecules interacting with CasL 3 (MICAL) family include five different genes (*MICAL1, 2, 3, L1, L2*) in mammals[38]. MICAL is a multidomain signal transduction protein that consists of a flavin adenine dinucleotide (FAD) - containing monooxygenase domain and domains for interacting with multiple proteins (Figure 6). The MICAL family of proteins has been shown to interact with several proteins including actin, Rab8, ELKS, collapsin response mediator protein 2 (CRMP2) and Plexins[39,40]. For example, MICAL

directly regulates actin reassembly in *Drosophila*, through its FAD-containing monooxygenase domain[41,42]. The FAD-containing monooxygenase domain of mammalian MICAL is required for its roles in Sema-dependent axon steering, axon guidance and synapse button definition in the nervous system, through the generation of H_2O_2, a reactive oxygen species (ROS)[43]. Sema3A stimulation activates the MICAL monooxygenase domain, which generates H_2O_2. This in turn induces Cys^{504} which leads to the disulfide-linked homodimer formation of CRMP2, and causes growth cone collapse[44]. However, the function of MICAL3 in cancer cells or stem cells is not fully understood.

When a stem cell divides into two daughter cells, there are two kinds of cell division; symmetrical and asymmetrical[45–47]. A stem cell produces two daughter cells by symmetric division, which doubles the number of self-renewing stem cells. In contrast, asymmetric cell division gives rise to two daughter cells, one of which is a differentiated cell and the other is a self-renewing stem cell. It has been reported that cancer cells with stem-like properties have a tendency to divide symmetrically, producing two daughter cancer stem cells, thus expanding the cancer stem population.

Numb plays an important role in the regulation of symmetric-asymmetric cell division in vertebrates[48,49](Figure 7). In *Drosophila*, the Numb protein is localized to the basal side of

neural stem cells in prophase[50]. Numb is expressed in differentiated cells and regulates asymmetric cell division. Conversely, in mammalian neural cells Numb protein is localized to one side of the cell membrane in dividing stem or progenitor cells[51,52]. When a neural stem cell or progenitor cell divides, the daughter cell that inherits the majority of the Numb protein self-renews, whereas the other cell that inherits a lower amount of Numb protein, differentiates to become a neuron. Other studies have reported that Numb induced asymmetric division in colon cancer stem cells by acting as a negative regulator of Notch signaling[53]. However, it remains largely unknown whether Numb has any role in BCSCs.

4. Material and Methods

Reagents and antibodies

For immunoblotting, anti-MICAL3 (H-56, 1:200, Santa Cruz Biotechnology), anti-Numb (C29G11, 1:1,000, Cell Signaling), anti-CRMP2 (C4G, 1:100, IBL) and anti-GAPDH (D23H3, 1:5000, Millipore) primary antibodies, and horseradish peroxidase (HRP)-conjugated anti-rabbit or anti-mouse IgG secondary antibodies were used. For immunostaining, an anti-Numb (1:100, Abcam) primary antibody and an Alexa 546 anti-mouse IgG antibody secondary antibody were used. For flow cytometry, Alexa fluor 647-labeled anti-CD24, APC-H7 labeled anti-CD44 anti-NP1 (446921, R&D Biosystems) conjugated antibodies were used. For the tumor sphere assay, an anti-NP1 primary antibody (446921, R&D Biosystems) was used.

Cell lines and primary cell culture

The mammary The mammary epithelial cell line, MCF10A, and the breast cancer cell lines, MCF7, T47D, BT20, BT474 and MDA-MB-436, were purchased from the American Type Culture Collection (ATCC). Cells were cultured in RPMI 1640 culture medium (Nacalai Tesque) containing, 10% fetal bovine serum (FBS; SAFC Biosciences), 100 units/ml penicillin and 100 µg/ml streptomycin (Nacalai Tesque).

Cultured Cell lines were cultured in a humidified atmosphere at 37°C in 5% CO_2 and the

culture medium was changed every 2 days. When cells reached subconfluence, they were rinsed in phosphate buffered saline (PBS) (pH 7.4, Nacalai Tesque) and trypsinized with 0.25% Trypsin-EDTA Solution (Nacalai Tesque) for 1 min at 37°C, and passaged at ratios of 1:3 ~ 1:5.

Isolated Isolation of single cells from breast tumor tissues

Patient-derived tumor tissues were cut into < 5 mm^3 pieces in PBS. A mechanical disaggregation system (Medimachine, Becton Dickinson) was used to obtain single-cell suspensions from the solid tumors. A Medicon (50 μm) device containing the tissues was inserted into the Medimachine (BD™ Medimachine) and subjected to a 1 min pulse. The resulting single-cell suspension was filtered through a 100-μm cell strainer (BD Falcon) and washed with PBS. In the case of disaggregated cell clusters, the single-cell suspension was incubated in Accumax (Innova Cell Technologies) at room temperature for 10 min.

Primary cell culture

To isolate Lin^- breast cancer cells, cells obtained from breast tumor specimens were incubated with a mixture of biotin-conjugated antibodies against Lin^+ cells. The antibody mixture included a MACS lineage kit for depletion of hematopoietic and erythrocyte precursor cells (CD2, CD3, CD11b, CD14, CD15, CD16, CD19, CD56, CD123 and CD235a,

Miltenyi Biotec), endothelial cells (CD31, eBioscience) and stromal cells (CD140b, Biolegend). After incubation, cells were separated using the MACS magnetic cell separation system according to manufacturer instructions (Miltenyi Biotec). Isolated lineage-negative (Lin^-) breast cancer cells were cultured in Human EpiCult™-B Medium Kit medium (Stem Cell Technologies) that includes a supplement mix, freshly-prepared 0.48 μg/ml hydrocortisone (Stem Cell Technologies), 2mM L-glutamine (Nacalai Tesque), 100 units/ml penicillin and 100 μg/ml streptomycin.

Isolated single cells were cultured in a humidified atmosphere at 37°C in 5% CO_2 and the culture medium was changed every 2 days. When cells reached subconfluence, they were rinsed in PBS, trypsinized with Accumax for 10 min at room temperature, and passaged at a ratio of 1:4.

Tumor sphere formation assay

I previously confirmed that patient-derived tumor cells plated at 5,000 cells/ml yield tumor spheres that are clonally derived from single cells. Cells were therefore plated as single cell suspensions in 24-well ultra-low attachment plates at a low density (5,000 cells/ml) to obtain single cell-derived tumor spheres. The cells were grown in sphere culture medium (SCM), which consists of serum-free Dulbecco's modified Eagle's Medium:Nutrient Mixture F-12 (DMEM/F-12) medium (GIBCO), 20 ng/ml EGF (Millipore), 20 ng/ml bFGF (PeproTech),

B27 supplement (GIBCO) and heparin (Stem Cell Technologies), as previously described. Alternatively, spheres were grown in DMEM/F-12 medium supplemented with 20 ng/ml recombinant human HRG (R&D Systems Inc.), 200 ng/ml recombinant human Sema 3A (R&D Systems Inc.) with or without anti-Neuropilin-1 antibody (clone R&D Systems Inc.). Spheres with a diameter of > 75 μm were counted after 4 to 7 days.

Construction of lentivirus vectors

For construction of the lentivirus plasmid vector for knock-down of the *MICAL3* gene, the short hairpin RNA (shRNA) sequence was inserted in the pENTR4-H1 vector (a kind gift from H. Miyoshi, RIKEN, Tsukuba, Japan) as an entry vector.

100μg The pENTR4-H1 vector containing the shRNA sequence (100 μg) and a lentiviral vector (150 ng/μl) (CS-RfA-EG) were used to perform recombination with a Gateway® LR Clonase® Enzyme mix (Invitrogen) containing a proteinase K solution according to manufacturer recommendations, to generate the shRNA expression clone.

Lentivirus plasmid DNA (1000 ng/μl) was transducted into HEK293FT cells along with packaging plasmids (pCMV-VSV-G-RSV-Rev and pCAGHIVgp) using the lipofectamine transfection reagent (Invitrogen) and PLUS™ Reagent (Invitrogen). The medium was changed after 16 h. High-titer viral stocks were prepared by ultracentrifugation.

Transduction of cells with lentiviral vectors

The culture supernatant containing infection-competent virus particles was applied to cultivated MCF7 cells or patient-derived breast cancer cells at a multiplicity of infection of 1:10, and was incubated for 24 hours at 37°C in 5% CO_2. After incubation, GFP positive cells were sorted using FACS Aria II (BD Bioscience).

Small interfering RNA (siRNA)

For knock-down of *MICAL3*, breast cancer cell lines (MCF7, T47D, BT474, BT20 and MBA-MB-467) or patient-derived breast cancer cells were seeded at a density of 1×10^5 cells/well onto a 6-well plate. After incubation for 24 hours, cells were added to ON-TARGETplus MICAL3 siRNA (GE Healthcare) and DharmaFECT transfection reagent (GE Healthcare) in serum-free medium. The control was an ON-TARGETplus Non-targeting siRNA.

For knock-down of *SEMA3B*, *CRMP2* and *Numb*, breast cancer cell lines were seeded at a density of 5×10^5 cells/well onto a 6-well plate and were incubated with Stealth RNAi™ (Invitrogen) and Lipofectamine™ RNAiMAX transfection reagent (Invitrogen) according to the manufacturer protocol. RNAi duplex (10 nM final concentration) and Lipofectamine™ RNAiMAX complexes were added to each well. The control was the Stealth™ RNAi Negative Control with low GC content.

SiRNA-transfected cells were incubated at 37°C in 5% CO_2 until the assay. Representative data from three independent experiments using two types of siRNA are shown.

Transiently transfection of plasmids

All expression vectors were a gift from Dr. Anna Akhmanova (Utrecht University, Utrecht, The Netherlands)[40]. We used the following described expression vectors: GFP-MICAL3, GFP-MICAL3-3G3W and GFP-MICAL3-N1. GFP-MICAL3 was generated from the human cDNA clone, pF1KA0819, using a modified pEGFP-C1 vector. GFP-MICAL3-3G3W and GFP-MICAL3-N1 were generated from GFP-MICAL3 using a PCR-based strategy. The control was a pEGFP-C1 vector.

For transient transfection of plasmids, breast cancer cell lines were seeded at a density of 3×10^5 cells/well onto a 6-well plate. After incubation for 24 hours, the plasmids (1.8 μg) and a PolyFect Transfection Reagent (Qiagen) in culture medium without antibiotics were added to each well.

Flow cytometry

Primary cells from breast cancer tissues or cultured cells were dissociated into single cells using Accumax and washed with PBS. To analyze the population of breast cancer stem cells, single cells were sorted after staining with Alexa flour 647-labeled anti-human CD24 and

APC-H7 labeled anti-human CD44 at 4°C for 20 min.

Dead cells were excluded using propidium iodide (PI) (Nacalai Tesque) staining. All flow cytometric analyses were performed with a FACS Aria II (BD Bioscience) and data were analyzed using FlowJo software (Treestar).

Immunoblotting

For sodium dodecyl sulfate polyacrylamide gel electrophoresis (SDS-PAGE), the cultured cells in 6-well plates were washed with PBS and then lysed with Lysis buffer containing RIPA Buffer (Pierce), a Phosphatase Inhibitor Cocktail (Nacalai Tesque) and a Protease Inhibitor Cocktail (Nacalai Tesque). For nonreducing SDS-PAGE, the cells were lysed in a buffer containing 15 mM iodoacetamide (IAA, Sigma) and 1% SDS and incubated for 30 min at 37°C to block further oxidation of cysteine residues[44].

The proteins Proteins were separated by SDS-PAGE and transferred to polyvinylidene fluoride (PVDF) membranes. The membranes were blocked with 5% skim milk in PBS and incubated with primary antibodies overnight at 4°C. After washing three times in PBS containing 0.1% Tween 20, the PVDF membranes were incubated with the appropriate secondary antibody at RT for 1 hour. Signals were developed using an Immobilon Western Chemiluminescent HRP Substrate (Millipore), and were examined using a LAS3000 (Fujifilm, Tokyo, Japan) imaging system.

Immunostaining

Cultured cells were fixed in 4% Paraformaldehyde/PBS (Nacalai Tesque) at room temperature (RT; 24°C) for 15 min. After washing in PBS containing 0.15 % Triton X-100 for 10 min, cells were incubated with 1% bovine serum albumin (Nacalai Tesque) at RT for 60 min to block nonspecific binding, and then were incubated with the primary antibody at 4℃, overnight. After washing with PBS, cells were incubated with the appropriate secondary antibodies at RT for 1 hour. Cells were coverslipped using glycerol containing DAPI (Sigma) to stain the nuclei, and examined under a fluorescence microscope (Carl Zeiss).

In situ Proximity Ligation Assays (PLA)

For the analysis of interactions with proteins, a Duolink® *in situ* Proximity Ligation Assay (Olink Bioscience) was used[54]. Cells were fixed in 4% Paraformaldehyde/PBS and washed with PBS containing 0.15 % Triton X-100 to permeabilize the cells. Cells were incubated overnight with the primary antibodies. After washing with PBS, both Probe marker PLUS (positive oligonucleotide) and MINUS (negative complementary oligonucleotide) were used as secondary antibodies. A detection reagent (red or green) was used to visualize protein interactions. The total number of signal dots was counted separately in the nucleus and the cytoplasm using a fluorescence microscope and analyzed using ImageJ.

Xenografts

Eight-week-old female immunodeficient NOD/scid gamma (NSG) mice were anesthetized with isofluorane (Abbott Japan). Ninety day-release β-estradiol (E2) pellets containing 0.72 mg of E2 (Innovative Research of America) were implanted subcutaneously into the back of the neck, before 3 days in cell implantation. For PDXs, breast cancer tissues obtained from breast cancer patients were cut into 1 mm squares and 5 pieces were suspended in Matrigel (BD Biosciences) to produce 50 μl of the cell mixture. Five pieces per site, or cells expressing the indicated constructs, were subsequently injected into the mammary fat pads of NSG mice. When tumors reached > 100 mm^3, the mice were killed. To distinguish between the human tumor cells and mouse cells in PDXs, FITC-labeled anti-mouse H-2Kd was used to label mouse MHC Class Ⅰ, and V450-labeled anti-rat CD45 (BD Pharmingen) was used to label mouse leukocytes, concurrently. The population excluding the H-2Kd and CD45 positive cells was isolated using flow cytometry. Tissue fragments were retransplanted into another cohort of mice. For limiting dilution assays (LDAs), cells were suspended in 50 μl Matrigel (BD Biosciences) and were injected subcutaneously into each mammary fat pad of NSG mice.

ELISA

To measure the level secreted Sema3B by SCM or HRG stimulation, a Human Semaphorin 3B ELISA Kit (Abbexa) was used. We collected culture supernatants from MCF7 cells treated

with SCM or HRG for 16, 24 and 48 hours. Culture supernatants were incubated in plate binding with a Sema3B antibody at 37℃ for 2 hours. After washing, a detection antibody and a HRP-conjugated antibody were incubated at 37℃ each. Absorbance at 560 nm was measured using a Wallac Victor 1420 multilabel counter (PerkinElmer).

H_2O_2 assay

The An Amplex red hydrogen peroxide/peroxidase assay kit (Invitrogen) was used to measure hydrogen peroxide production from the purified enzymatic domain of MICAL3 as previously described[43,55]. For cell lysate experiments, HEK293FT cells (1×10^6 cells) transfected with GFP-fusion constructs were lysed using 120 μl lysis buffer containing 20 mM HEPES (pH 7.4), 100 mM NaCl, 1% NP-40 and Protease Inhibitor Cocktail. After incubation at 4℃, lysates were cleared by centrifugation. Reactions were performed in a 100 μl volume, consisting of 50 μl of the cell lysate, 200 μM NADPH, Amplex red reagent (10-acetyl-3,7-dihydroxyphenoxazine), and 0.1 U/ml horseradish peroxidase (HRP) in reaction buffer. 1 μM H_2O_2 was used as a positive control. Absorbance at 560 nm was measured using a Wallac Victor 1420 multilabel counter.

Quantitative real-time (qRT)-PCR

Total RNA was prepared using the TRIzol Reagent (Invitrogen) and was transcribed into

cDNA using a High Capacity cDNA Reverse Transcription kit (Applied Biosystems). Quantitative RT-PCR was performed using TaqMan probes from Applied Biosystems, according to manufacturer recommendations.

Microarray experiments

Cells were serum-starved for 16 hours prior to stimulation with heregulin (HRG) (100 ng/ml). DHMEQ (1 μg/ml) or LY294002 (1 μg/ml) was added 2 hours prior to HRG stimulation. Total RNA was isolated every hour for up to 16 hours after each treatment using TRIzol reagent (Life technologies). Alternatively, cells overexpressing IGF2 or control vector-transduced cells were trypsinized and the single cell suspension was incubated overnight. Total RNA was subsequently isolated using the TRIzol reagent. All samples showed RNA Integrity Numbers (RIN) greater than 9.5 and were subjected to microarray experiments according to manufacturer instructions. Total RNA samples (100 ng) were labeled with Cyanine 3-CTP using a Low Input Quick Amp Labeling Kit (Agilent Technologies). Hybridization was carried out using a Gene Expression Hybridization Kit (Agilent Technologies) as follows: 1.65 mg of cRNA samples were fragmented (30 min at 60℃) and were then hybridized to a 4x180K Agilent Whole Human genome Oligo DNA Custom Microarray (G4862A, Agilent Technologies). The array includes 46,117 unique probes that were designed to identify transcripts of coding and predicted non-coding genes

including long intergenic non-coding RNAs (lincRNA). Microarrays were scanned using a dynamic autofocus microarray scanner (Agilent DNA Microarray Scanner, Agilent Technologies) under default parameters (Green PMT was set to 100%, and the scan resolution was set to 5 μm). Feature Extraction Software v9.1 (Agilent Technologies) was used to obtain a raw signal value and a quality flag (Present [P], Marginal [M], or Absent [A]). After aggregating all the scanned signals for the different time points, a parametric empirical Bayes approach called ComBat was used to remove non-biological experimental variation or batch effects (52). A 75 percentile normalization was then applied to remove between-experiment distributional biases due to assay artifacts. To reduce outliers' effects, signal values were further smoothed for each gene under each condition by a moving average of length 3 with equal weights.

Identification of gene sets up-regulated by the HER2/3—PI3K—NFκB pathway at early time points up to 6 hours and throughout the time course

In order to identify genes downstream of HER2/3—PI3K—NF-κB pathway at early time points after stimulation (up to 6 hours), we first calculated average gene expression profiles at the seven measured time points (0, and every hour thereafter) under each condition of the study (N, no treatment; D, treatment with DHMEQ [NF-κB inhibitor]; LY, treatment with LY294002 [PI3K inhibitor]; H, stimulation with HRG; HD, stimulation with HRG and

treatment with DHMEQ; and HLY, stimulation with HRG and treatment with LY294002). The potentially up-regulated genes downstream of HER2/HER3-PI3K-NFkB pathway at early time points were selected based on the following criteria: Hj ≧1.25 Nj (Nj/Hj≦0.8), Hj ≧ 1.25 Dj (Dj/Hj≦0.8), Hj ≧1.25 LYj (LYj/Hj≦0.8), Hj ≧1.11 HDj (HDj/Hj≦0.9), Hj ≧ 1.11 HLYj (HLYj/Hj≦0.9). Fifty-seven transcripts were selected. A similar type of analysis was used to identify candidate genes downstream of HER2/3-PI3K-NF-κB pathway throughout the time course (from 0 hours to 16 hours). One hundred and eighty-nine transcripts were selected. Raw and normalized microarray data are available from the Gene Expression Omnibus (GEO) database (accession numbers GSE64073).

Study approval

All human breast carcinoma specimens were obtained from the University of Tokyo Hospital, Minami Machida Hospital and Showa General Hospital. This study was approved by the institutional review boards of the Institute of Medical Science, University of Tokyo, the University of Tokyo Hospital, Minami Machida Hospital and Showa General Hospital (24－29－1207). Written informed consent was received from all the participants prior to inclusion in the study. Mice were handled according to the guidelines of the Institute of Medical Science, University of Tokyo. The experiments were approved by the committees for animal research at the Institute of Medical Science, University of Tokyo.

Statistics

Student's The student's unpaired *t*-test was used to compare differences between two samples and values of $p < 0.01$-0.05 (*), $p < 0.001$-0.01 (**) or $p < 0.001$(***) were considered significant. Values are presented as means ± SD. For sphere assay, the spheres were counted and the percentage of sphere forming cells was determined for each group. LDAs of frequency determinations, as well as the corresponding p values, were generated using ELDA software, which took into account whether the assumptions for LDA were met (http://bioinf.wehi.edu.au/software/elda/index.html, provided by the Water and Eliza Hall Institute[56].

5. Results

Sema3B and MICAL3 are downstream targets of the HER2/3-PI3K-NFκB pathway

In order to identify genes that are potentially regulated by HER2/3-PI3K-NFκB signaling, I examined the gene expression profile of MCF7 breast cancer cells upon stimulation with HRG, in the presence or absence of DHMEQ and LY294002, which are specific inhibitors of NFκB and PI3K, respectively. I selected a dose of 1 μg/ml for DHMEQ and 1 μM for LY294002, as these have been previously shown to cause ~50% inhibition of HRG-induced tumor sphere formation[23] (Figure 4A). Upon stimulation with growth factors, the changes in gene expression levels over time are highly dynamic. I examined expression levels every hour for up to 16 hours after stimulation (Figure 4B). My criteria for candidate genes were that their expression levels were increased following stimulation with HRG, but were reduced by treatment with the inhibitors. Because I obtained data from many time points, I considered the differences in expression levels to be significant, even if only < 1.5-fold at each time point. Among the upregulated genes were several growth factors, cytokines and their receptors, including *Sema3B* and its downstream target *MICAL3* (Figure 4B), both of which are related to Sema signaling. These results suggest that Sema3B and MICAL3 are downstream targets of HER2/3-PI3K-NFκB pathway in breast cancer cells (Figure 28).

Sema3s are key factors of tumor sphere formation of human breast cancer cells

Sema3B was one of the downstream targets of HER2/3-PI3K-NFκB signaling identified from the DNA microarray (Figure 8A) and high levels of Sema3B expression correlated with a poor prognosis obtained from Prognoscan (http://www.abren.net/PrognoScan/) (Figure 8B). I first confirmed the existence of secreted Sema3B in the culture supernatant in SCM or following HRG stimulation using ELISA (Figure 8C). I next evaluated tumor sphere formation in Sema3B knockdown MCF7 cells using Sema3B siRNA (Table3 and Figure 8D). A reduction in secreted Sema3B significantly decreased tumor sphere formation in SCM or following HRG stimulation (Figure 8E).

When Sema3A was the only growth factor present, it induced tumor sphere formation in luminal type MCF7 and basal type BT20 cells (Figure 9A and B). These results suggest that type 3 Semas, including Sema3A and 3B, play an important role in tumor sphere formation in an autocrine or paracrine manner.

Expression of *MICAL3* correlates with poor prognosis in breast cancer patients

Using a DNA microarray, I identified MICAL3 as one of the downstream targets of HER2/3-PI3K-NFκB signaling (Figure 10A). To determine whether expression of *MICAL3* is upregulated in patient-derived breast cancer tissues, I examined its expression in breast cancer tissues using the Oncomine cancer gene expression database (http://www.oncomine.com). I

found that *MICAL3* expression was higher in breast cancer tissues than in normal breast tissue (Figure 10B). I next determined the correlation between MICAL3 expression and prognosis using PrognoScan and showed that MICAL3 expression in breast cancer tissues can be classified into high- and low-expressing groups. The high MICAL3-expression groups displayed a significantly reduced distant metastasis free survival (DMSF) and relapse free survival (RFS), compared with the low MICAL3-expression group (Figure 10C). These results indicate that breast cancer patients with tumors that express high levels of MICAL3 show a poor prognosis.

MICAL3 induces stem-like properties in breast cancer cells

To elucidate the function of MICAL3 in BCSCs, I first evaluated the tumor sphere-forming ability of human breast cancer cell lines and patient-derived primary breast cancer cells. To knockdown MICAL3, cells were transfected with SMART pool siRNA (Figure 11A). MICAL3 knockdown decreased sphere forming ability in many breast cancer cell lines, including luminal type MCF7, HER2-positive type BT474, basal A type BT20 and basal B type MBA-MB-436 cells (Figure 11B). I also studied MICAL3 knockdown using two different siRNAs corresponding to non-overlapping sequences in MICAL3 (Figure 12A and B) and showed that MICAL3 knockdown decreased sphere forming ability in MCF7 and BT20 cell lines (Figure 12C). Next, I analyzed patient-derived primary breast cancer cells and

found that MICAL3 knockdown suppressed the tumor sphere forming ability of patient-derived breast cancer cells (Figure 1A and B).

Tumor-initiating activity is another measure of cancer stem cell properties. I generated MICAL3 stable knockdown cells using a MICAL3 variant 1 shRNA (Table 1 and Figure 14A). I confirmed that MICAL3 knockdown suppressed tumor sphere forming ability in MCF7 cells in vitro by transducing them with MICAL3 shRNA (Figure 14B). I next inoculated these cells into the mammary fat pads of immunocompromised IL2-receptor γc-deficient (NSG) mice. An estimate of the tumor-initiating cell frequency was much lower in MICAL3 variant 1 knockdown cells than in control cells (1/7,115 *vs.* 1/49,833, $P = 0.0383$; Figure 14C). Tumor weight 30 days after transplantation was significantly decreased in MICAL3 variant 1 knockdown cells, compared to control cells (Figure 14D). This finding indicates that the MICAL3 variant 1 has strong tumor-initiating activity. To assess tumorigenicity for MICAL3 using primary breast cancer cells, I established MICAL3 stable knockdown cells using two different shRNAs for MICAL3, corresponding to non-overlapping sequences (Figure 15A). When I inoculated these cells into the mammary fat pads of NSG mice, tumor-initiating activity was strongly inhibited in both MICAL3 knockdown cells (#1, 1/10 vs. 1/490, $P = 2.01e-08$; #2, 1/10 vs. 1/56, $P = 0.0122$;Figure 15B and C). These results indicate that MICAL3 plays an important role in tumor sphere formation in vitro and in tumor-initiating activity in vivo, both in breast cancer cell lines and in primary breast cancer cells.

Monooxygenase domain of MICAL3 has a key role for tumor sphere forming ability

MICAL3 contains a FAD-containing monooxygenase domain, a calponin homology (CH) domain, LIM domain and a coiled-coil domain[57] (Figure 16A). To determine which of these domains is required for tumor sphere formation in breast cancer cells, I used two DNA constructs, MICAL3-3G3W and MICAL3-N1 (Figure 16A). MICAL3-3G3W is a dominant-negative MICAL3 mutant in which the three glycines in the FAD binding motif GXGXXG were mutated to tryptophans. This triple mutation was shown to abrogate the function of *Drosophila* MICAL in axon guidance and actin disassembly[41,57]. MICAL3-N1 lacks the C-terminal region containing the coiled-coil domain, which contributes to vesicle fusion to the plasma membrane[40]. I transfected each construct into HEK293FT cells then measured levels of H_2O_2 production in the presence of 200 μM NADPH using an enzyme-linked assay[43,55,58] (The Amplex red hydrogen peroxide/peroxidase assay kit; Figure 16B). Cells transfected with wild-type MICAL3 (MICAL3-WT) produced higher levels of H_2O_2 than controls (Figure 16C). In contrast, MICAL3-3G3W produced much lower levels of H_2O_2 than MICAL3-WT or MICAL3-N1. It has been reported that the MICAL1 C-terminal region has an autoinhibitory function in monooxygenase activity in the N-terminal region. However, our results showed that MICAL3-N1 produced comparable levels of H_2O_2 to wild-type MICAL3. This finding indicates that the N-terminal region of MICAL3 does not inhibit the production of H_2O_2.

I next analyzed tumor sphere formation in MCF7 cells that were transiently transfected with those constructs. When transfected cells were floating cultured in SCM and with Sema3A stimulation, both MICAL3-WT and MICAL3-N1 were able to induce tumor sphere formation (Figure 16D and E). However, tumor sphere forming ability was greatly inhibited in MICAL3-3G3W transfected cells. These results indicate that the monooxygenase domain of MICAL3 promotes tumor sphere formation by producing H_2O_2 in human breast cancer stem cells.

MICAL3 increases cancer stem-like properties through CRMP2 dimerization

It is known that MICAL forms a complex with PlexA, a receptor for Sema signal, and the LIM domain of MICAL contributes to CRMP interaction[43]. I next investigated the interaction between MICAL3 and CRMP2 using a Duolink® in situ Proximity Ligation Assay (PLA)[54]. In situ PLA is a technique used to detect interactions between proteins inside a cell, and uses fluorescein to generate valuable images (Figure 17A). In situ PLA is different from conventional FRET / BRET and co-immunoprecipitation, and it is possible to detect the interaction and localization of endogenous protein as spots visualized by microscopy. When MCF7 cells were treated with SCM or Sema3A for 24 hours, the number of PLA dots was increased in SCM- or Sema3A-stimulated cells (Figure 17B, C). In particular, a significant number of PLA dots were detected in Sema3A-stimulated cells (Figure 17C). These results

indicate that SCM or Sema3A stimulation induced the interaction between MICAL3 and CRMP2 in human breast cancer cells.

To examine whether CRMP2 is involved in tumor sphere formation in human breast cancer cells, MCF7 cells were transfected individually with two different CRMP2 siRNAs (Table 3 and Figure 18A). CRMP2 knockdown cells showed remarkably decreased tumor sphere formation in SCM or following Sema3A stimulation (Figure 18B and C).

I next examined whether dimerization of CRMP2 is induced by MICAL3-mediated ROS activation in human breast cancer cells. I treated MCF7 cells with 1 μM H_2O_2 and loaded the total lysates onto nonreducing SDS-PAGE. I found that intensities of the bands around 135 kD, corresponding to the disulfide-linked homodimers of CRMP2, were increased following treatment with H_2O_2 (Figure 19A). When MCF7 cells were stimulated with Sema3A, the intensities of the bands around 135 kD, corresponding to the homodimers of CRMP2, were increased (Figure 19B). Furthermore, MICAL3 knockdown using shRNA dramatically reduced the intensities of the bands of the homodimers of CRMP2 (Figure 19C). These results suggest that dimerization of CRMP2 is induced by MICAL3-mediated ROS activation in human breast cancer cells.

MICAL3-mediated ROS production induces an interaction between CRMP2 and Numb

CRMP2 is known to directly interact with the amino-terminal fragment containing the PTB

domain of Numb during axon growth in the nervous system[59–61]. To examine whether CRMP2 interacts with Numb in breast cancer cells following Sema3A stimulation, I used in situ PLA. MCF7 cells were transfected with MICAL3 siRNA and then treated with growth factors (SCM) or Sema3A for 24 hours. The number of PLA dots was markedly increased following treatment with SCM or Sema3A. MICAL3 knockdown significantly decreased the number of PLA dots induced by SCM or Sema3A treatment (Figure 20A and B). To determine whether the monooxygenase domain of MICAL3 is required for the interaction between CRMP2 and NUMB, I transfected MCF7 cells with MICAL3-WT or 3G3W and then treated the cells with growth factors (SCM) or Sema3A for 24 hours. The number of PLA dots was greatly reduced in MICAL3-3G3W transfected cells, compared to MICAL3-WT transfected cells (Figure 21A and B). These results indicate that the monooxygenase domain of MICAL3 is required for the interaction between CRMP2 and Numb following treatment with SCM or Sema3A (Figure 27).

Numb increases cancer stem-like properties in Sema3A-stimulated breast cancer cells via MICAL3

I next analyzed the amount of Numb protein using immunoblotting. Stimulation with Sema3A increased the amount of Numb protein, whereas MICAL3 knockdown remarkably decreased the amount of Numb protein (Figure 22A). When I transiently transfected the cells

with cDNA constructs (control vector, MICAL3-WT, 3G3W or N1), the amount of Numb protein was increased in cells expressing MICAL3-WT or N1, but not in cells expressing MICAL3-3G3W (Figure 22B). To investigate whether Numb is involved in tumor sphere formation, MCF7 cells were transfected individually with two types of Numb siRNA (Figure 22C). Tumor sphere formation was remarkably decreased in Numb knockdown cells treated with SCM or Sema3A (Figure 22D). These results indicate that Sema3-induced activation of the monooxygenase domain of MICAL3 induces CRMP2 dimerization and the interaction between CRMP2 and Numb, and then stabilizes Numb protein for tumor sphere formation.

NP1 is expressed in a BCSC-enriched population and plays an important role in tumor sphere formation

I found that NP1 was overexpressed in several human breast cancer cells compared to MCF10A cells, a normal human mammary epithelial cell line (Figure 23A). In order to examine the mechanisms by which Sema3 functions in breast cancer stem cells, I analyzed NP1 expression in a $CD44^{high}CD24^{low}$ cell population that is enriched for BCSCs. I found that NP1 was more strongly expressed in the BCSC-enriched population than in the other cell population (Figure 23B). Moreover, the expression levels of NP1 were variable in the $CD44^{+}$ cell population (Figure 24A and B). I then sorted patient-derived primary breast cancer cells using an anti-NP1 antibody to obtain cell populations in which NP1 was expressed at either

high or low levels. When I analyzed tumor sphere forming ability in these sorted cells, the $NP1^{high}$ cell population, but not the $NP1^{low}$ cell population, gave rise to spheres (Figure 24C). I next analyzed sphere formation in the presence of a NP1 neutralizing antibody (NAb). Patient-derived primary breast cancer cells were sorted using the anti-NP1 antibody to obtain the $NP1^{high}$ cell population (Figure 25 A). Then cells were treated with SCM in the presence of the NP1 NAb. Tumor sphere formation was greatly inhibited by the NP1 NAb (Figure 25 B and C), indicating that cells with cancer stem-like properties express high levels of NP1.

MICAL3 promotes symmetric division of NP1 positive-cancer stem like cells through stabilization of Numb

To analyze symmetric-asymmetric cell division, I performed a cell pair assay using patient-derived breast cancer cells (Figure 26A). NP1-positive cells were isolated from patient-derived breast cancer cells and were cultured at a low density for 24 hours. I then changed the medium to SCM or medium containing Sema3A and continued to culture. FBS-containing medium was used as a control. After 24 hours, single NP1-positive cells divided into pairs of daughter cells that were stuck together (Figure 26B). When patient-derived breast cancer cells were co-immunostained with anti-NP1 and anti-Numb antibodies after the first cell division, the NP1-positive cells co-localized with the Numb protein on the cell membrane or in the cytoplasm (Figure 26B). In symmetrically-divided

cells, the Numb protein was strongly expressed and localized to both daughter cells. In asymmetrically-divided cells, the Numb protein was expressed in only one of the daughter cells, and was localized at the region where the cell was attached to the other daughter cell. Interestingly, NP1 was co-expressed in the Numb-positive daughter cell but not in Numb-negative daughter cell. When treated with SCM, 56% of cell divisions were symmetric, producing two NP1-positive daughter cells, and 44% were asymmetric, producing one NP1-positive daughter cell and one NP1-negative daughter cell (Figure 26C). These results suggest that SCM treatment gives rise to more undifferentiated daughter cells by symmetric cell division. I next investigated whether the type of cell division was altered by MICAL3 knockdown. The results of a cell paired assay showed that both SCM and Sema3A induced asymmetric division during the first cell division of a NP1-positive cell (Figure 27A and B). In contrast, MICAL3 knockdown markedly increased asymmetric division. This result is consistent with the finding that MICAL3 promotes symmetric division of a NP1-positive BCSC after SCM or Sema3A stimulation, which increases tumor sphere forming activity in NP1-positive BCSC (Figure 29).

6. Discussion

In the current study, I provide evidence that the Sema3/NP1/MICAL3/CRMP2/ NUMB axis presents a novel mechanism for the maintenance of symmetric division of self-renewing BCSCs to expand, at the expense of asymmetric cell division. To my knowledge, this is the first report describing the molecular mechanisms that underlie how a cancer stem cell population expands by symmetric division.

I used DNA microarray analysis to show that both *Sema3B* and *MICAL3* are downstream targets of the HER2/HER3-PI3K-NFκB pathway. The NFκB transcription factor complex can activate Sema signaling by inducing the expression of both a Sema3B ligand and the cytoplasmic signaling protein MICAL3, leading to self-renewal of BCSCs. Since expression levels of MICAL3 are up-regulated in breast cancer tissues compared to normal breast tissues, these represent cancer stem cell-specific mechanisms that control symmetric-asymmetric division, and therefore it should be possible to target these key molecules and eradicate cancer stem cells.

I found that Sema3A and Sema3B are key ligands of Sema signaling in cancer stem cells to promote self-renewal during the first cell division. Sema3B was found in a DNA microarray analysis of MCF7 cells treated with HRG, and was evaluated under HRG stimulation though

the HER2/3-PI3K-NFκB signaling pathway. Sema3A is secreted from the tumor microenvironment containing endothelial cells, and is expressed in different cell lines. Therefore, self-renewal of BCSC is accelerated by Sema3A and Sema3B secreted from different components within the tumor microenvironment, specifically in the cancer stem cell niche, in an autocrine or paracrine manner.

Cancer stem cells generally have been thought to maintain low levels of ROS, resulting in a resistance to anticancer drugs or radiation[62–64]. In contrast, it is reported that ROS plays important roles for mediating intercellular signals in cancer stem cells in some cases. For example, Rac1-driven ROS generation is essential for the effect of APC loss on $Lgr5^{+}$-intestinal stem cells and progenitors[65]. ROS signaling in the cancer stem cells is critical for tumorigenesis. My data suggest that ROS, generated by the monooxygenase domain of MICAL3 by stimulated with Sema3A, is critical for the symmetric division of self-renewing cancer stem cells. ROS forms a disulfide-linked homodimer of CRMP2 and the homodimerized CRMP2 then appears to stabilize the Numb protein. This is the first evidence that Sema3-stimulated ROS production maintains the self-renewal of cancer stem cells, through increased stability of the Numb protein. In this case, I consider that ROS is a key factor to contribute to BCSCs maintenance.

NP1 is a receptor for Sema3A and Sema3B and forms a complex with Plexins, transducers of Sema signaling in the steady state. A Sema signal causes the formation of a complex with MICAL3 and CRMP2 though the NP1/Plexin receptor complex[43]. Using in situ PLA, I showed that Sema3A stimulation promoted the interaction between MICAL3 and CRMP2 in breast cancer cells. Moreover, NP1 was expressed specifically in a BCSC-enriched population in patient-derived breast cancer cells. The fact that NP1-positive cells but not NP-negative cells induced tumor sphere formation suggests the strong association between NP1 expression and cancer stemness. These results suggest that Sema signaling is significantly activated in NP1 positive cells for inducing cancer stemness. I have concluded that NP1 positive cells may be an important marker of BCSCs.

It has been reported that CRMP and Numb regulate centrosome movements by asymmetric division of sensory progenitors in *Drosophila*[66]. However, it remains unproven whether Numb is related to the maintenance of stemness, or to Notch signaling in cancer stem cells. I found that Numb is necessary for tumor sphere formation, meaning that Numb participates in the self-renewal of BCSCs. Moreover, by interacting with CRMP2 homodimers formed by H_2O_2 production via MICAL3, Numb works together with NP1-positive cells during the first cell division. This finding that Numb may be an independent regulator of Notch signaling in cancer stem cell division is important for understanding cancer stem cell biology.

Drugs that target specific molecules may be used to eradicate cancer cells with stem-like properties, and may lead to a cure, by preventing recurrence of the disease. However, it is possible that a single drug will not sufficiently break the cancer stemness circuits. In the current study, I provide a rationale for using a combination of several targeted drugs involved in Sema signaling to regulate symmetric-asymmetric division. We found that MICAL3 knockdown inhibited tumor sphere formation and tumorigenicity in vivo and that Sema3A-induced tumor spheres were reduced by a neutralizing antibody against NP1. Thus, molecules involved in MICAL3-mediated Sema signaling, and specifically Semas and NP1, could be good candidates for the therapeutic treatment of breast cancer. If and when such target molecules related to Sema signaling are used in breast cancer therapy, it will be important to develop detectable predictive biomarkers to select responsive patients at the early stage of breast cancer. To this end, I think that it would be worth examining Sema3 protein levels in breast cancer tissues or blood samples, as a liquid biopsy, of breast cancer patients. However, this would need to be validated by examining a larger number of patients in a future study.

7. Acknowledgements

東京大学医科学研究所分子療法分野の東條有伸教授には指導教官として本研究の実施の機会を与えて戴き、その遂行にあたって御指導をいただいたことに、深謝の意を表します。

本研究にあたり直接の御指導を戴いた金沢大学がん進展制御研究所分子病態研究分野教授の後藤典子先生に深謝の意を表します。

東大病院乳腺・内分泌外科の多田敬一郎准教授、西岡琴江先生をはじめとする先生方、公立昭和病院乳腺・内分泌外科の金内一先生、同病理診断科の清水誠一郎先生、南町田病院の矢野正雄先生、獨協医科大学乳腺センターの小川利久教授、辻英一先生には、本研究で用いた乳がん臨床検体の提供に関してご尽力いただき、深く感謝申し上げます。

ユトレヒト大学 Dr. Anna Akhmanova には貴重な MICAL3 発現ベクター、コントロールベクターを提供して戴いたことに謝意を表します。

NFκB 阻害剤 DHMEQ を提供していただいた愛知医科大学分子標的医薬探索寄附講座の梅澤一夫教授に感謝申し上げます。

Flow cytometroy を使用した実験は東京大学医科学研究所 FACS コアラボラトリーの石井有実子技術職員、藤田梓技術職員の御協力無しでは遂行できませんでした。ここに感謝の意を表します。

最後に、東大医科学研究所分子療法分野分子標的研究グループの町田雪乃さん、木村奈津子さん、笹原麻子先生、村山貴彦さん、小宮由紀子さん、また、東京大学医科学研究所の皆さま、金沢大学がん進展制御研究所分子病態研究分野の皆さま、東大白金ひまわり保育園の皆さま、家族、友人にはさまざまな御支援、御協力を頂き、深く御礼申し上げます。

8. Reference

1. Perou, C. M. *et al.* Molecular portraits of human breast tumours. *Nature* **406,** 747–752 (2000).

2. Goldhirsch, A. *et al.* Personalizing the treatment of women with early breast cancer: highlights of the St Gallen International Expert Consensus on the Primary Therapy of Early Breast Cancer 2013. *Ann. Oncol.* **24,** 2206–2223 (2013).

3. Parkinson, D. R. *et al.* Evidence of clinical utility: an unmet need in molecular diagnostics for patients with cancer. *Clin. Cancer Res.* **20,** 1428–44 (2014).

4. England, T. N. Use of Chemotherapy Plus a Monoclonal Antibody Against Her2. *English J.* **344,** 783–792 (2001).

5. Thompson, Ian M, Lucia, M. S. *et al.* Trastuzumab after Adjuvant Chemotherapy in HER2-Positive Breast Cancer. 2239–2246 (2004). doi:10.1056/NEJMoa1212772

6. Hanrahan, E. O., Valero, V., Gonzalez-Angulo, A. M. & Hortobagyi, G. N. Prognosis and management of patients with node-negative invasive breast carcinoma that is 1 cm or smaller in size (stage 1; Tla,bN0M0): A review of the literature. *J. Clin. Oncol.* **24,** 2113–2122 (2006).

7. Magee, J. a, Piskounova, E. & Morrison, S. J. Cancer stem cells: impact, heterogeneity, and uncertainty. *Cancer Cell* **21,** 283–96 (2012).

8. Magee, J. A., Piskounova, E. & Morrison, S. J. Cancer Stem Cells: Impact,

Heterogeneity, and Uncertainty. *Cancer Cell* **21,** 283–296 (2012).

9. Hinohara, K. & Gotoh, N. Inflammatory signaling pathways in self-renewing breast cancer stem cells. *Curr. Opin. Pharmacol.* **10,** 650–4 (2010).

10. Borovski, T., De Sousa, E. M. F., Vermeulen, L. & Medema, J. P. Cancer stem cell niche: the place to be. *Cancer Res* **71,** 634–639 (2011).

11. Singh, a & Settleman, J. EMT, cancer stem cells and drug resistance: an emerging axis of evil in the war on cancer. *Oncogene* **29,** 4741–51 (2010).

12. Cabrera, M. C. Cancer stem cell plasticity and tumor hierarchy. *World J. Stem Cells* **7,** 27 (2015).

13. Al-Hajj, M., Wicha, M. S., Benito-Hernandez, A., Morrison, S. J. & Clarke, M. F. Prospective identification of tumorigenic breast cancer cells. *Proc. Natl. Acad. Sci. U. S. A.* **100,** 3983–8 (2003).

14. Keller, P. J. *et al.* Defining the cellular precursors to human breast cancer. (2011). doi:10.1073/pnas.1017626108/-/DCSupplemental.www.pnas.org/cgi/doi/10.1073/pnas.1017626108

15. Maguer-Satta, V., Chapellier, M., Delay, E. & Bachelard-Cascales, E. CD10: a tool to crack the role of stem cells in breast cancer. *Proc. Natl. Acad. Sci. U. S. A.* **108,** E1264; author reply E1265 (2011).

16. Islam, M. S. & Zhou, H. Isolation and characterization of putative epidermal stem cells

derived from Cashmere goat fetus. *Eur. J. Dermatol.* **17,** 302–8 (2007).

17. Lo, P.-K. *et al.* CD49f and CD61 identify Her2/neu-induced mammary tumor-initiating cells that are potentially derived from luminal progenitors and maintained by the integrin-TGFβ signaling. *Oncogene* **31,** 2614–26 (2012).

18. Wright, M. H. *et al.* Brca1 breast tumors contain distinct CD44+/CD24- and CD133+ cells with cancer stem cell characteristics. *Breast Cancer Res.* **10,** R10 (2008).

19. Farnie, G. & Clarke, R. B. Mammary stem cells and breast cancer--role of Notch signalling. *Stem Cell Rev.* **3,** 169–175 (2007).

20. Lamb, R. *et al.* Wnt Pathway Activity in Breast Cancer Sub-Types and Stem-Like Cells. *PLoS One* **8,** e67811 (2013).

21. Cordenonsi, M. *et al.* The Hippo transducer TAZ confers cancer stem cell-related traits on breast cancer cells. *Cell* **147,** 759–72 (2011).

22. Zhou, J. *et al.* Activation of the PTEN/mTOR/STAT3 pathway in breast cancer stem-like cells is required for viability and maintenance. *Proc. Natl. Acad. Sci. U. S. A.* **104,** 16158–63 (2007).

23. Hinohara, K. *et al.* ErbB receptor tyrosine kinase/NF-κB signaling controls mammosphere formation in human breast cancer. *Proc. Natl. Acad. Sci. U. S. A.* **109,** 6584–9 (2012).

24. Okabe, H. *et al.* CD44s signals the acquisition of the mesenchymal phenotype required

for anchorage-independent cell survival in hepatocellular carcinoma. *Br. J. Cancer* **110,** 958–66 (2014).

25. Cagnoni, G. & Tamagnone, L. Semaphorin receptors meet receptor tyrosine kinases on the way of tumor progression. *Oncogene* **33474,** 4795–4802 (2014).

26. Tessier-lavigne, M. & Goodman, C. The molecular biology of axon guidance.pdf. (1996).

27. Bagnard, D., Lohrum, M., Uziel, D., Püschel, a W. & Bolz, J. Semaphorins act as attractive and repulsive guidance signals during the development of cortical projections. *Development* **125,** 5043–5053 (1998).

28. Rohm, B., Ottemeyer, A., Lohrum, M. & Püschel, A. W. Plexin/neuropilin complexes mediate repulsion by the axonal guidance signal semaphorin 3A. *Mech. Dev.* **93,** 95–104 (2000).

29. Kruger, R. P., Aurandt, J. & Guan, K.-L. Semaphorins command cells to move. *Nat. Rev. Mol. Cell Biol.* **6,** 789–800 (2005).

30. Capparuccia, L. & Tamagnone, L. Semaphorin signaling in cancer cells and in cells of the tumor microenvironment--two sides of a coin. *J. Cell Sci.* **122,** 1723–1736 (2009).

31. Neufeld, G. & Kessler, O. The semaphorins: versatile regulators of tumour progression and tumour angiogenesis. *Nat. Rev. Cancer* **8,** 632–45 (2008).

32. Neufeld, G., Sabag, A. D., Rabinovicz, N. & Kessler, O. Semaphorins in angiogenesis

and tumor progression. *Cold Spring Harb. Perspect. Med.* **2,** a006718 (2012).

33. Gaur, P. *et al.* Role of class 3 semaphorins and their receptors in tumor growth and angiogenesis. *Clin. Cancer Res.* **15,** 6763–6770 (2009).

34. Staton, C. a *et al.* Expression of class 3 semaphorins and their receptors in human breast neoplasia. *Histopathology* **59,** 274–82 (2011).

35. Müller, M. W. *et al.* Association of axon guidance factor Semaphorin 3A with poor outcome in pancreatic cancer. *Int. J. Cancer* **121,** 2421–2433 (2007).

36. Luchino, J. *et al.* Semaphorin 3E Suppresses Tumor Cell Death Triggered by the Plexin D1 Dependence Receptor in Metastatic Breast Cancers. *Cancer Cell* **24,** 673–685 (2013).

37. Man, J. *et al.* Sema3C promotes the survival and tumorigenicity of glioma stem cells through Rac1 activation. *Cell Rep.* **9,** 1812–26 (2014).

38. Zhou, Y., Gunput, R.-A. F., Adolfs, Y. & Pasterkamp, R. J. MICALs in control of the cytoskeleton, exocytosis, and cell death. *Cell. Mol. Life Sci.* **68,** 4033–44 (2011).

39. Hung, R.-J. & Terman, J. R. Extracellular inhibitors, repellents, and semaphorin/plexin/MICAL-mediated actin filament disassembly. *Cytoskeleton (Hoboken).* **68,** 415–33 (2011).

40. Grigoriev, I. *et al.* Rab6, Rab8, and MICAL3 cooperate in controlling docking and fusion of exocytotic carriers. *Curr. Biol.* **21,** 967–74 (2011).

41. Hung, R.-J. *et al.* Mical links semaphorins to F-actin disassembly. *Nature* **463,** 823–7 (2010).

42. Hung, R.-J., Pak, C. W. & Terman, J. R. Direct redox regulation of F-actin assembly and disassembly by Mical. *Science* **334,** 1710–3 (2011).

43. Schmidt, E. F., Shim, S.-O. & Strittmatter, S. M. Release of MICAL autoinhibition by semaphorin-plexin signaling promotes interaction with collapsin response mediator protein. *J. Neurosci.* **28,** 2287–97 (2008).

44. Morinaka, A. *et al.* Thioredoxin mediates oxidation-dependent phosphorylation of CRMP2 and growth cone collapse. *Sci. Signal.* **4,** ra26 (2011).

45. Morrison, S. J. & Kimble, J. Asymmetric and symmetric stem-cell divisions in development and cancer. *Nature* **441,** 1068–1074 (2006).

46. Neumüller, R. a & Knoblich, J. a. Dividing cellular asymmetry: asymmetric cell division and its implications for stem cells and cancer. *Genes Dev.* **23,** 2675–99 (2009).

47. Knoblich, J. a. Mechanisms of asymmetric stem cell division. *Cell* **132,** 583–97 (2008).

48. Shen, Q., Zhong, W., Jan, Y. N. & Temple, S. Asymmetric Numb distribution is critical for asymmetric cell division of mouse cerebral cortical stem cells and neuroblasts. *Development* **129,** 4843–4853 (2002).

49. Shimojo, H., Ohtsuka, T. & Kageyama, R. Dynamic Expression of Notch Signaling Genes in Neural Stem/Progenitor Cells. *Front. Neurosci.* **5,** 1–7 (2011).

50. Noatynska, A., Tavernier, N., Gotta, M. & Pintard, L. Coordinating cell polarity and cell cycle progression: what can we learn from flies and worms? *Open Biol.* **3,** 130083 (2013).

51. Zhong, W. & Chia, W. Neurogenesis and asymmetric cell division. *Curr. Opin. Neurobiol.* **18,** 4–11 (2008).

52. Dzierzak, E. & Enver, T. Stem cell researchers find their niche. *Development* **135,** 1569–1573 (2008).

53. Suzuki, T. *et al.* MICAL, a novel CasL interacting molecule, associates with vimentin. *J. Biol. Chem.* **277,** 14933–41 (2002).

54. Söderberg, O. *et al.* Direct observation of individual endogenous protein complexes in situ by proximity ligation. *Nat. Methods* **3,** 995–1000 (2006).

55. Zhou, Y. *et al.* MICAL-1 Is a Negative Regulator of MST-NDR Kinase Signaling and Apoptosis. *Mol. Cell. Biol.* **31,** 3603–3615 (2011).

56. Hu, Y. & Smyth, G. K. ELDA: Extreme limiting dilution analysis for comparing depleted and enriched populations in stem cell and other assays. *J. Immunol. Methods* **347,** 70–78 (2009).

57. Terman, J. R., Mao, T., Pasterkamp, R. J., Yu, H.-H. & Kolodkin, A. L. MICALs, a family of conserved flavoprotein oxidoreductases, function in plexin-mediated axonal repulsion. *Cell* **109,** 887–900 (2002).

58. Nadella, M., Bianchet, M. a, Gabelli, S. B., Barrila, J. & Amzel, L. M. Structure and activity of the axon guidance protein MICAL. *Proc. Natl. Acad. Sci. U. S. A.* **102,** 16830–16835 (2005).

59. Nishimura, T. *et al.* CRMP-2 regulates polarized Numb-mediated endocytosis for axon growth. *Nat. Cell Biol.* **5,** 819–26 (2003).

60. Arimura, N., Menager, C., Fukata, Y. & Kaibuchi, K. Role of CRMP-2 in neuronal polarity. *J. Neurobiol.* **58,** 34–47 (2004).

61. Schmidt, E. F. & Strittmatter, S. M. The CRMP family of proteins and their role in Sema3A signaling. *Adv. Exp. Med. Biol.* **600,** 1–11 (2007).

62. Ishimoto, T. *et al.* CD44 Variant Regulates Redox Status in Cancer Cells by Stabilizing the xCT Subunit of System xc− and Thereby Promotes Tumor Growth. *Cancer Cell* **19,** 387–400 (2011).

63. Kobayashi, C. I. & Suda, T. Regulation of reactive oxygen species in stem cells and cancer stem cells. *J. Cell. Physiol.* **227,** 421–430 (2012).

64. Diehn, M. *et al.* Association of reactive oxygen species levels and radioresistance in cancer stem cells. *Nature* **458,** 780–783 (2009).

65. Myant, K. B. *et al.* ROS production and NF-??B activation triggered by RAC1 facilitate WNT-driven intestinal stem cell proliferation and colorectal cancer initiation. *Cell Stem Cell* **12,** 761–773 (2013).

66. Jauffred, B. *et al.* Regulation of centrosome movements by Numb and the Collapsin Response Mediator Protein during Drosophila sensory progenitor asymmetric division. *Development* **140,** 2657–2668 (2013).

10. Figure

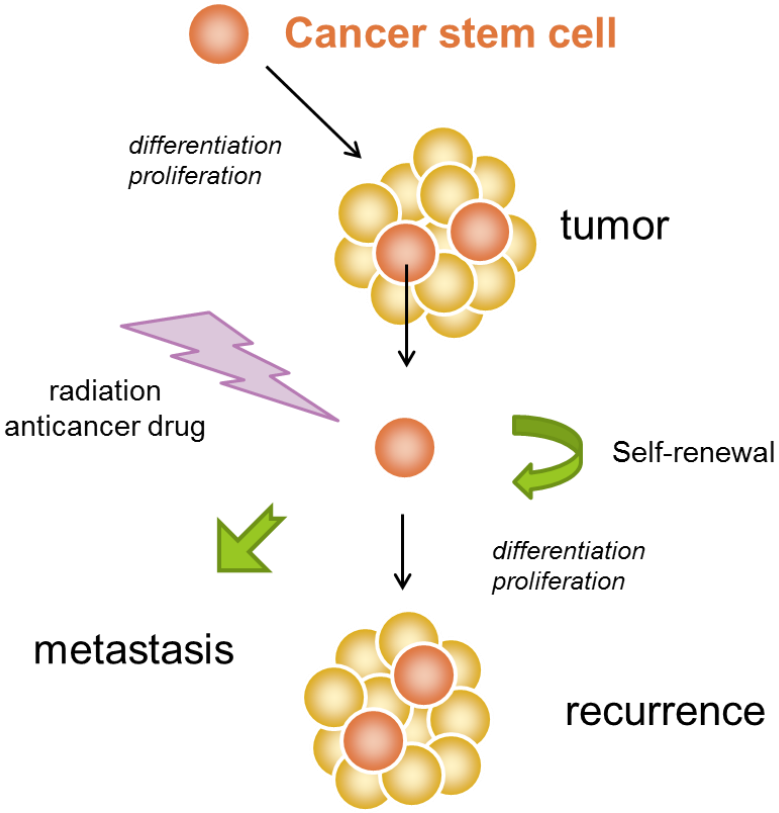

Figure 1

The concept of cancer stem cells

The cancer stem cells are few cells in tumor, but contain high tumorigenicity. Those cells have self-renewal capacity and resistance to radiation and anticancer drug. Even when large population of cancer cells are killed by anticancer drug, only a few cancer stem cells may survive and cause tumor recurrence and metastasis.

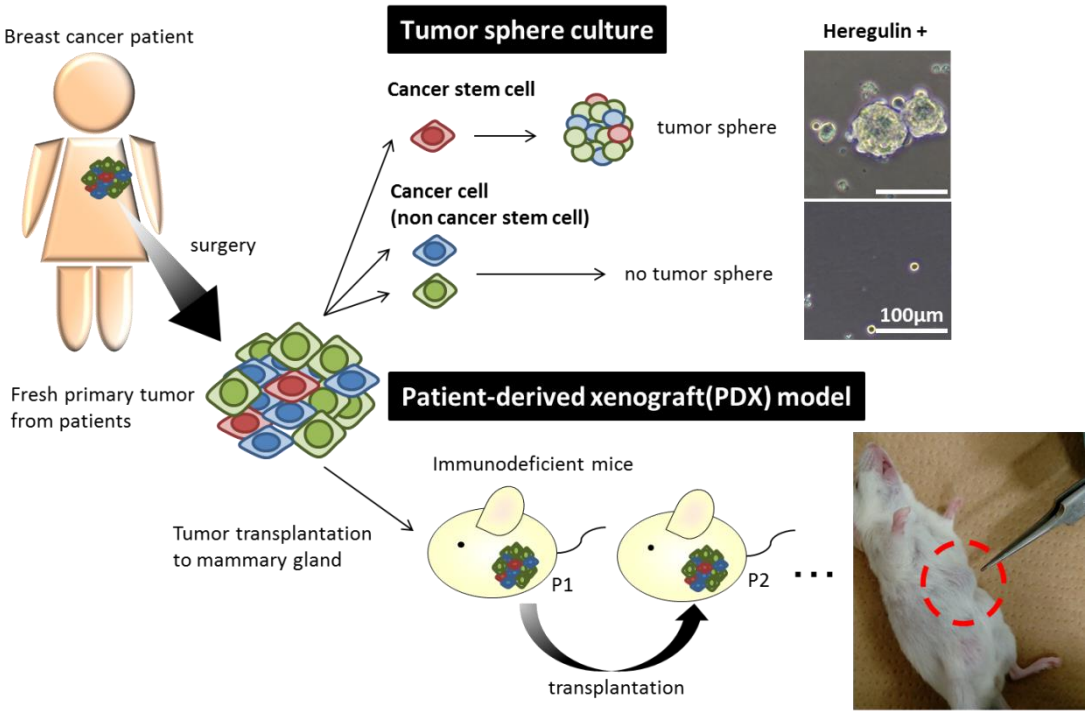

Figure 2

Methods to study cancer stem cells

Sphere forming activity in breast cancer stem cells (BCSC)-enriched population derived from fresh cancer cells of breast cancer patients. Tumor sphere forming ability is a property of cancer stem cells. **Patient-derived xenografts (PDXs)** are transplantable tumors grown from the patient-derived breast cancer cells in mammary tissues of the immune-deficient mice.

A

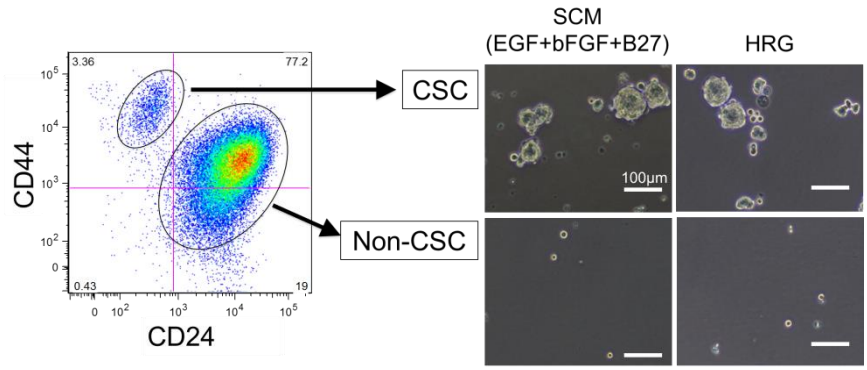

B

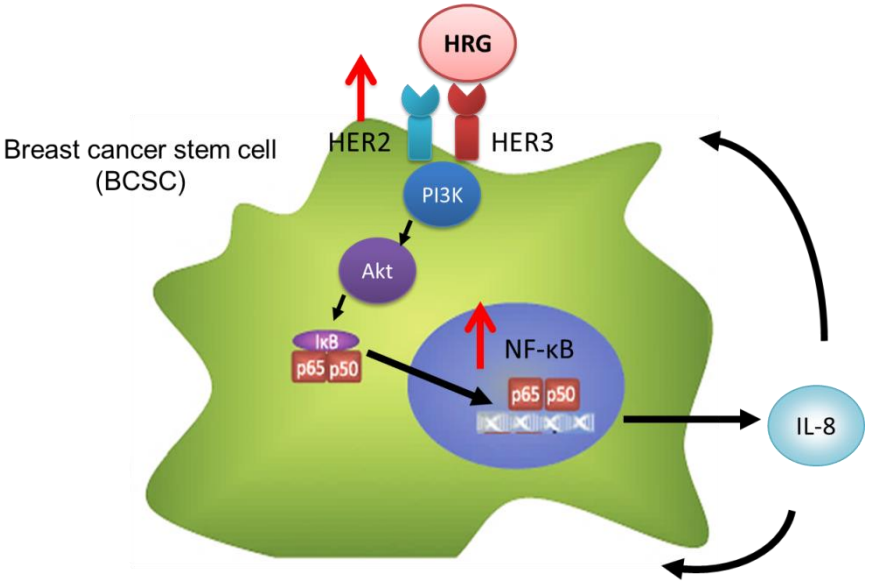

Figure 3

Potential inflammatory signaling pathways in BCSCs

(A) The sphere forming activity in cancer stem population derived from fresh cancer cells of breast cancer patients. Tumor spheres can grow from cancer stem cell-enriched population but not from non-cancer stem cell population. Tumor sphere formation is induced by treatment with heregulin (HRG) or a cocktail of growth factors and hormones contained in sphere culture medium (SCM), including EGF, bFGF and B27. (B) HRG, a ligand of HER3, plays important roles for tumor sphere formation of breast cancer stem cells through PI3K-NFκB pathway.

A

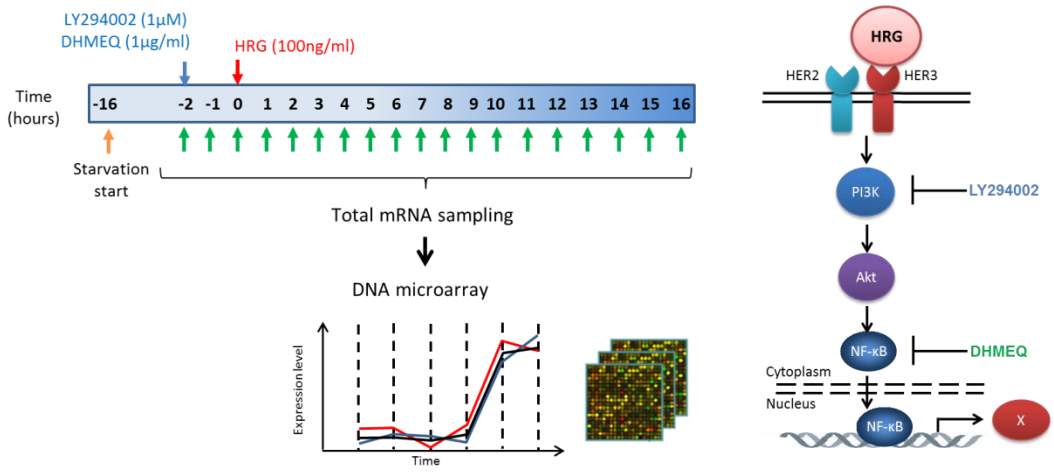

B

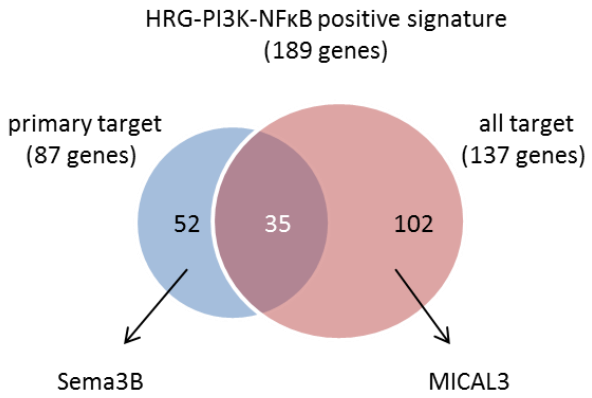

Figure 4

MICAL3 and Semaphorin3B (SEMA3B) are downstream targets of HRG-PI3K-NFκB pathway.

(A) An experimental procedure of DNA microarray analysis. (B) A Venn diagram showed downstream targets of HRG-PI3K-NFκB pathway that were upregulated at early time points (primary target, up to 6 hours) and/or throughout the time course (all target, 0-16 hours) after HRG treatment.

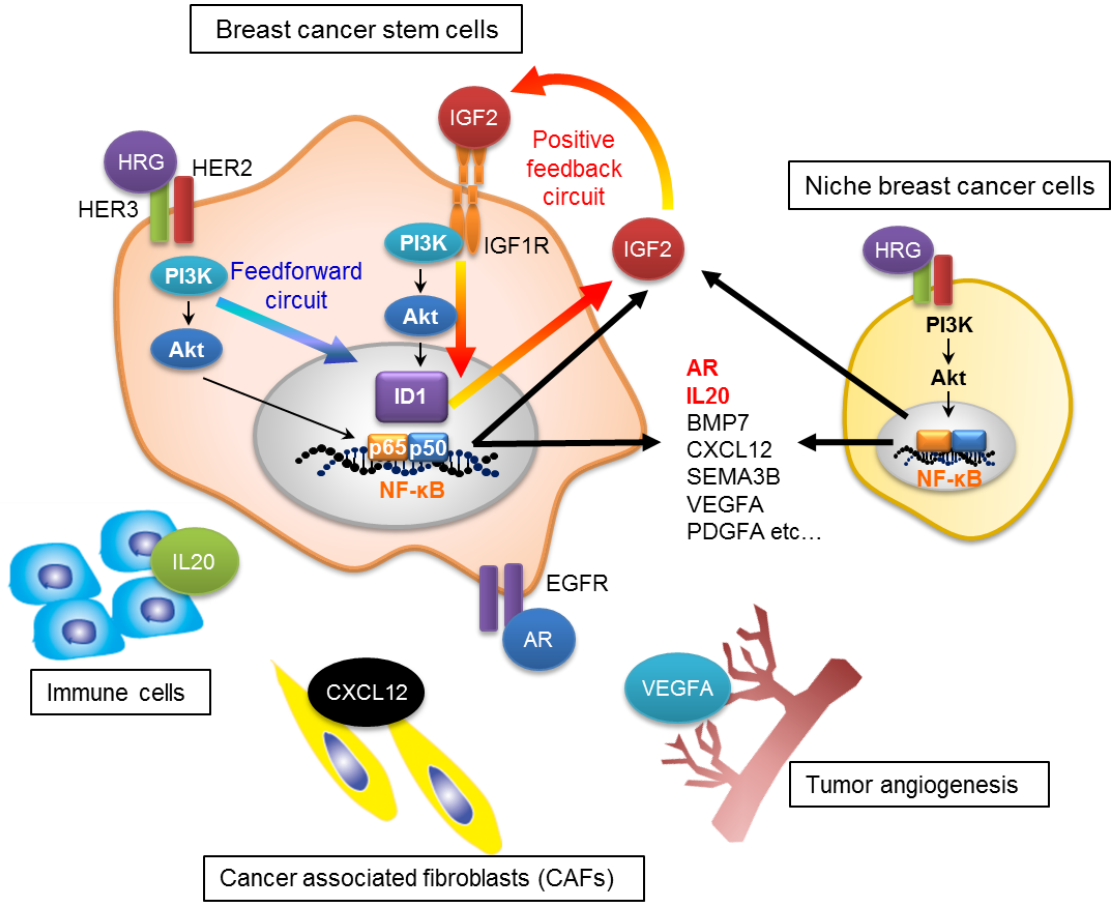

Figure 5

Model of molecular mechanisms that stabilize the stemness of cancer cells.

HER2/HER3-PI3K-NFκB pathway may trigger IGF2-PI3K-ID1-IGF2 positive feedback circuit (orange arrows) and PI3K-mediated feed-forward circuit (blue arrow) as fundamental mechanisms of stabilization of the stemness state. In addition, HER2/HER3-PI3K-NFκB pathway also leads to the production of many soluble factors that may regulate the surrounding niche cells: cancer cells, cancer associated fibroblasts (CAFs), endothelial cells, pericytes and immune cells.

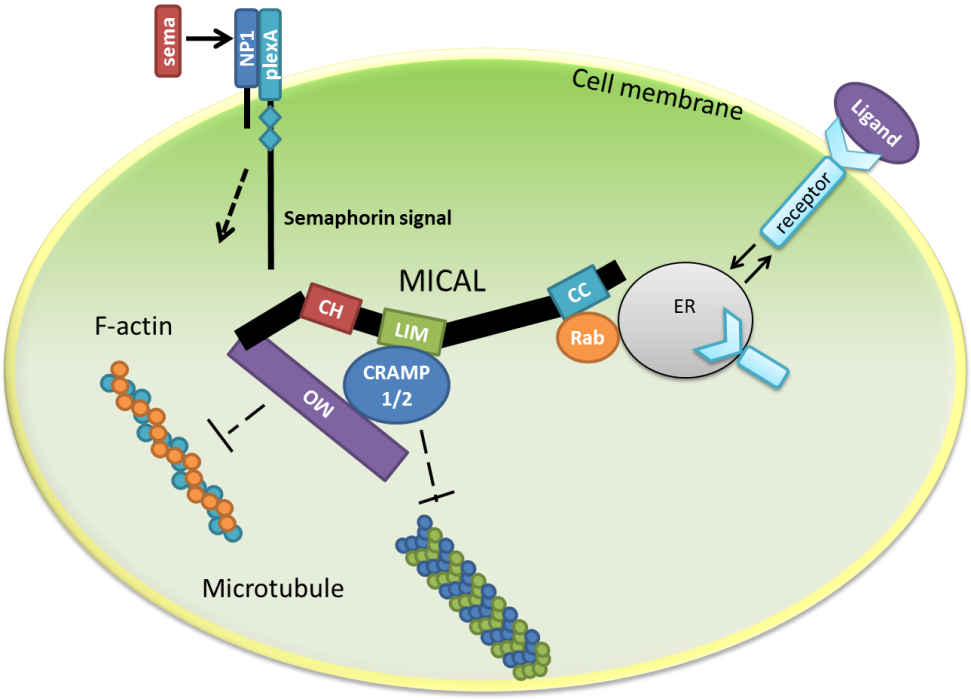

Figure 6

Signaling through MICAL protein

MICAL is a multidomain signal transduction protein containing an N-terminal FAD-containing monooxygenase-like domain, and interacts with multiple proteins involved in vesicle fusion to the plasma membrane and the cytoskeleton disassembly.

MO, monooxygenase; CH, calponin homology domain; LIM, Lin11, Isl-1, Mec-3 domain (zinc binding); CC, coiled-coil domain

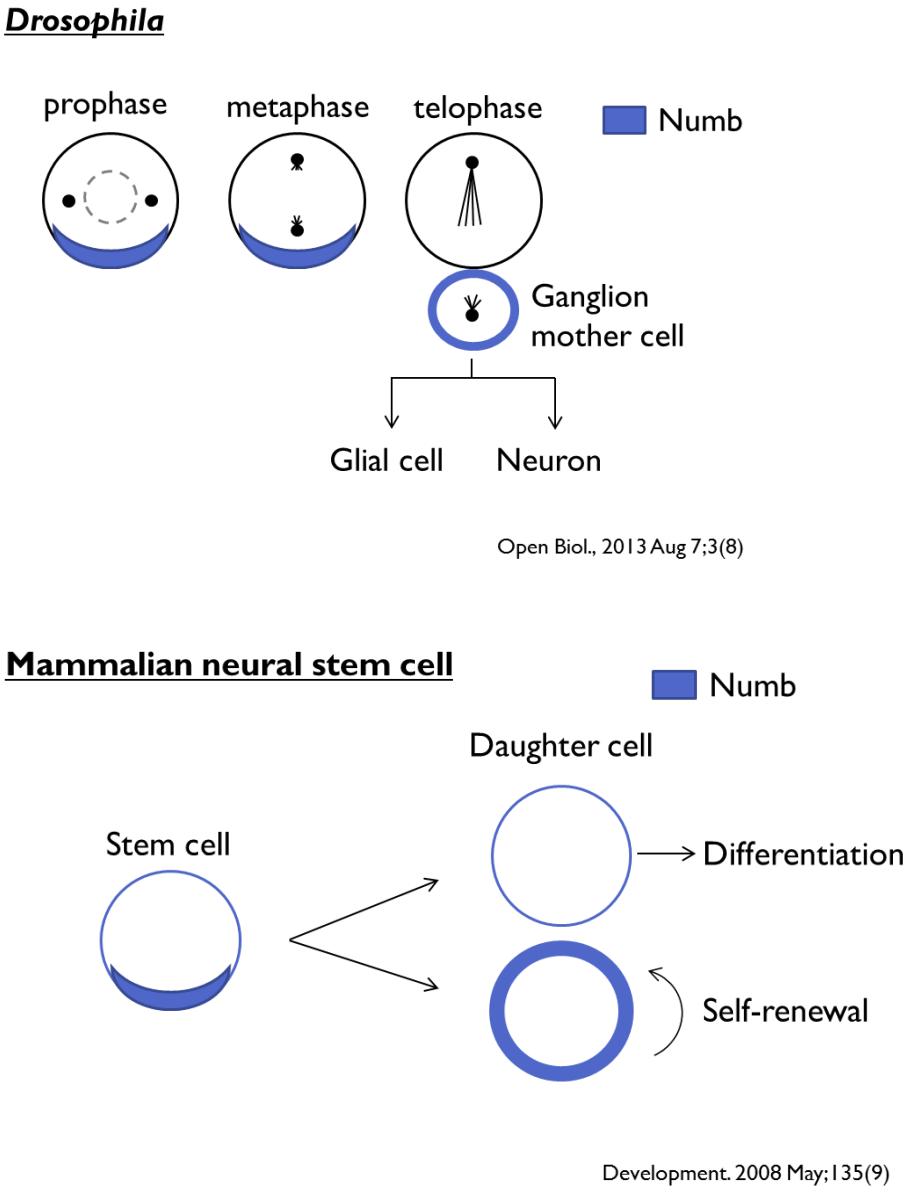

Figure 7

Numb regulation of symmetric-asymmetric cell division

Expression of Numb regulates self-renewal or differentiation of neural stem cells in *Drosophila* (Upper) and mouse (Lower).

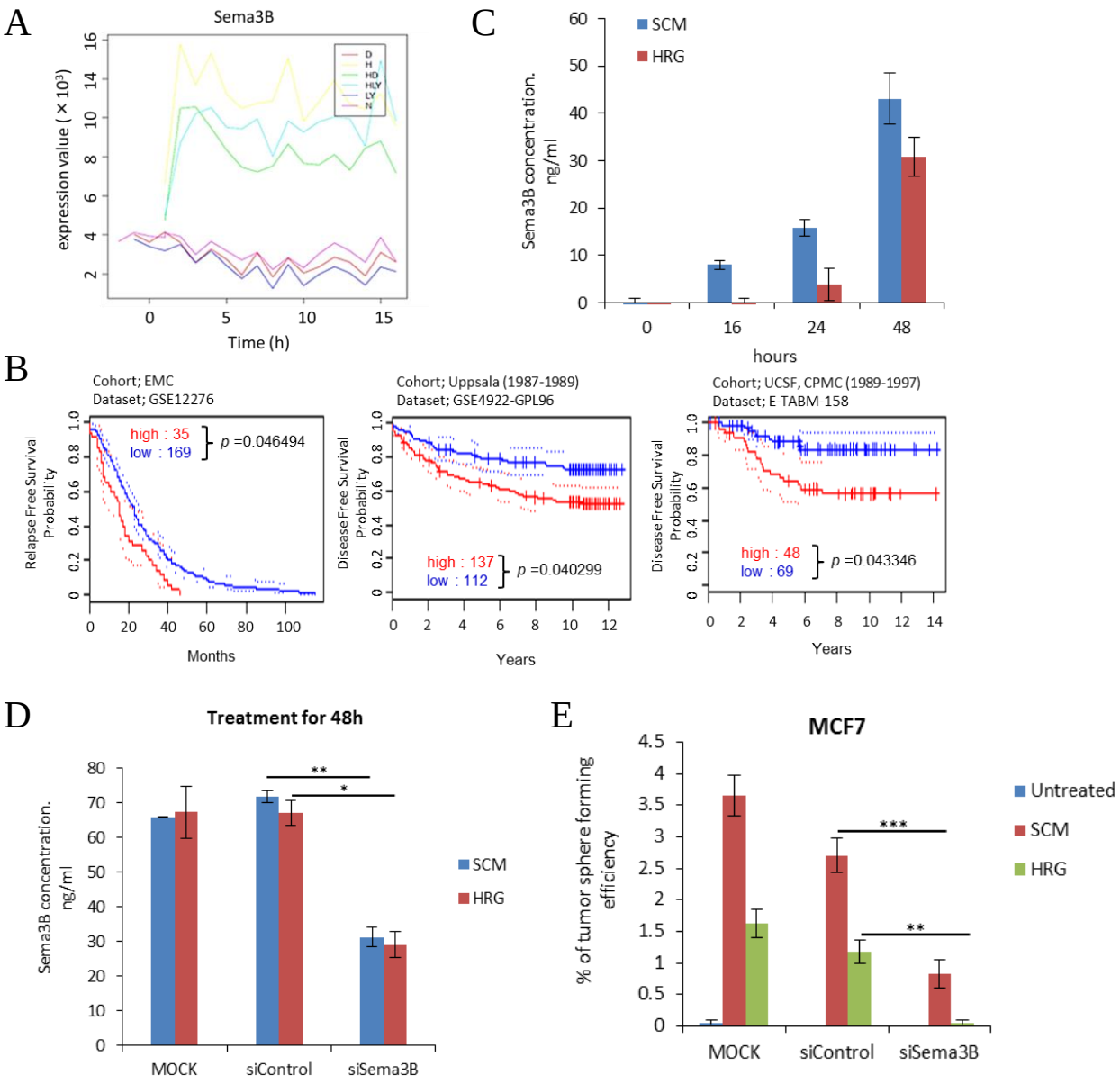

Figure 8

Sema3B secreted by SCM or HRG treatment, participate in sphere forming activity in MCF7 cells.

(A) Time-course expression patterns of *Sema3B* mRNA by microarray analysis in MCF7 cells after treatment with HRG (H) w/wo LY294002 (LY) and DHMEQ (D). (B) Kaplan-Meier plots for estimation of relapse free survival and disease free survival of patients with breast cancer tissues showing low or high *Sema3B* expression analyzed by Prognoscan. (C) Production of Sema3B in culture media was examined using ELISA upon stimulation with HRG or SCM. n = 3. (D) Production of Sema3B in culture media was reduced by knock-down of *Sema3B*. (E) SCM or HRG-induced tumor sphere formation of MCF7 cells was reduced by knock-down of *Sema3B*. n = 4.

A

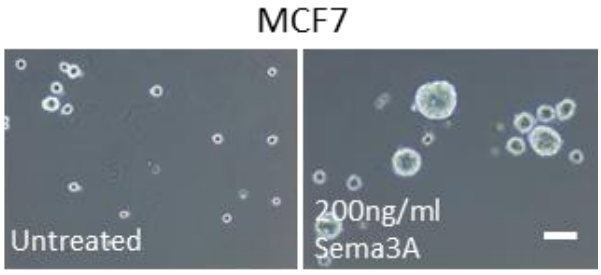

B

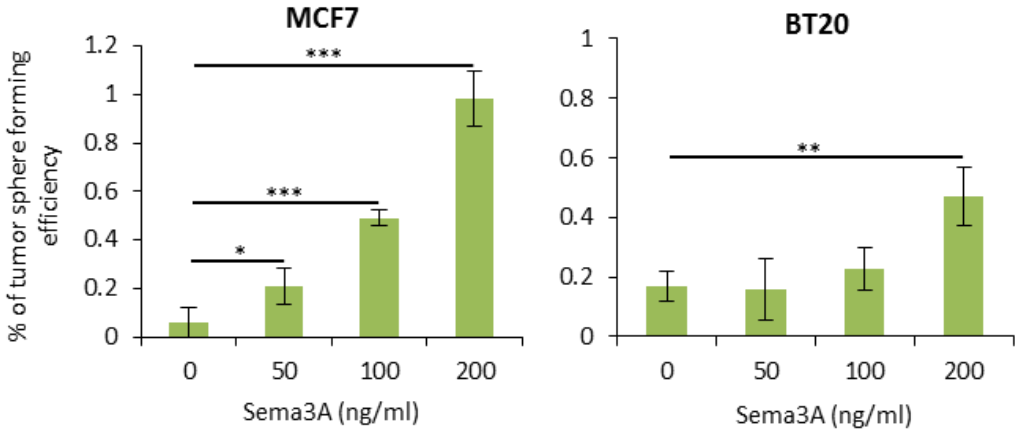

Figure 9

Sema3A treatment induces sphere forming activity in MCF7 cells

(A) Representative phase contrast images of formed tumor spheres of MCF7 cells treated with recombinant human Sema3A. Scale bar: 100 μm. (B) Tumor sphere formation of MCF7 cells (Luminal type, left panel) and BT20 cells (Basal type, right panel) increased by treatment of Sema3A.

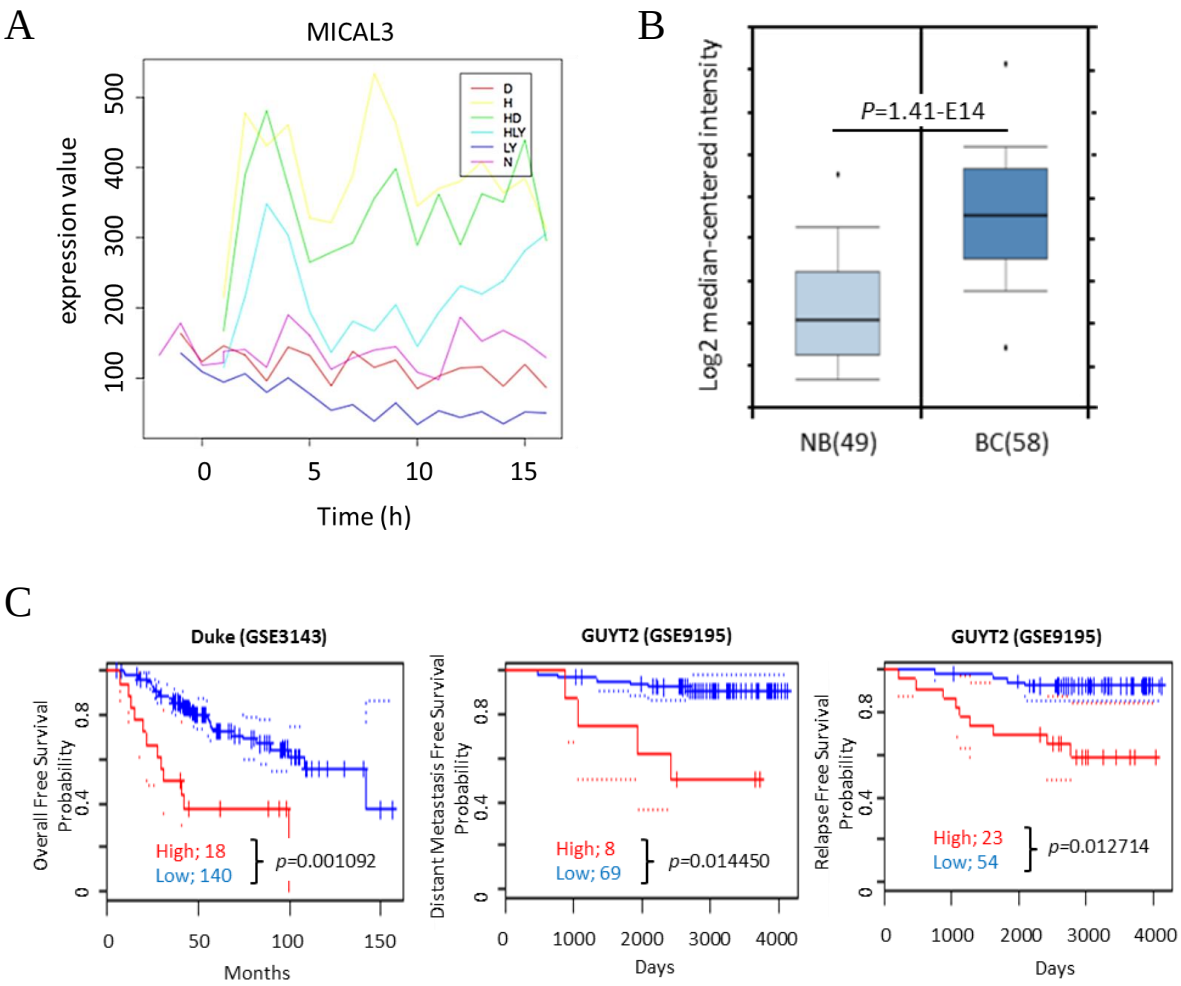

Figure 10

Expression of *MICAL3* is induced by HRG in breast cancer cells and correlation of *MICAL3* expression in breast cancer tissues with prognosis of the patients

(A) Time-course expression patterns of *MICAL3* mRNA by microarray analysis in MCF7 cells after treatment with HRG (H) w/wo LY294002 (LY) and DHMEQ (D). (B) Comparison of expression levels of *MICAL3* mRNA in normal breast (NB) and breast cancer (BC) tissues using Oncomine databases. (C) Kaplan-Meier plots for estimation of overall survival, distant metastasis free survival and relapse free survival of patients with breast cancer tissues showing low or high *MICAL3* expression analyzed by Prognoscan.

A

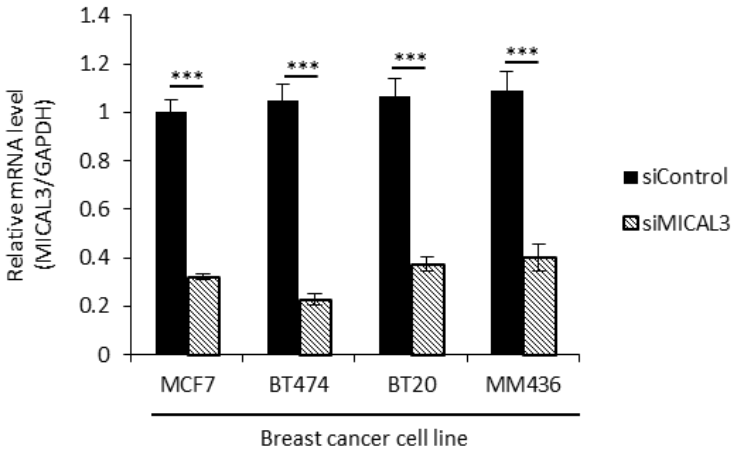

B

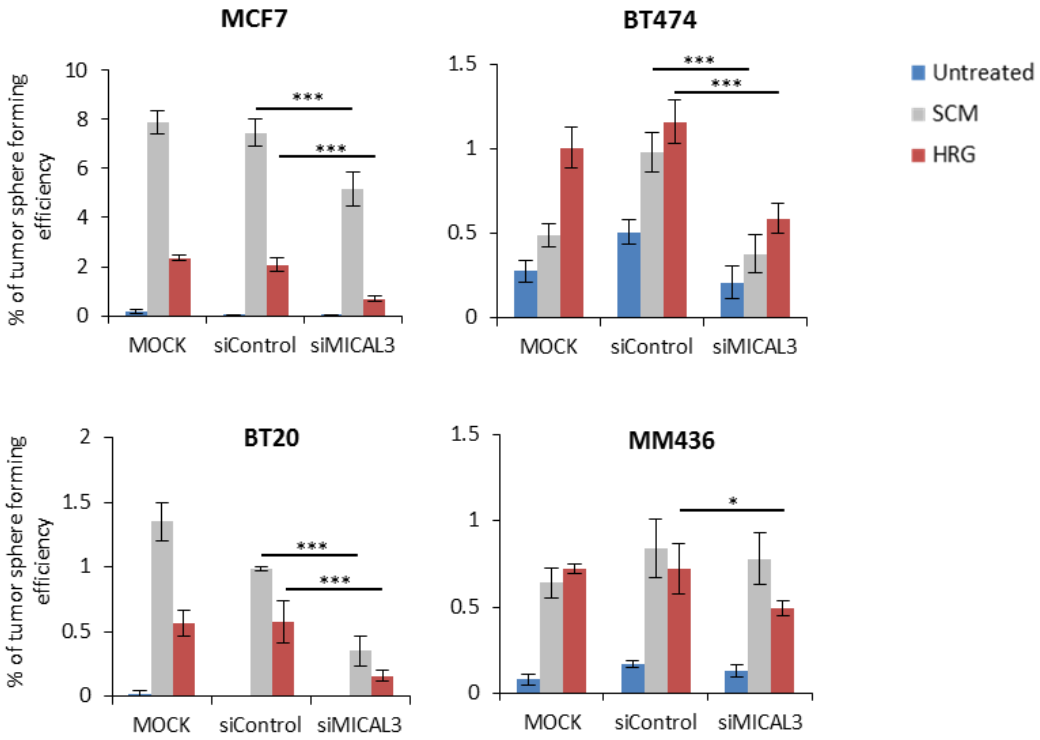

Figure 11

MICAL3 is a key factor for tumor sphere formation of human breast cancer cell lines.

(A) Expression of *MICAL3* mRNA by qRT-PCR in MCF7 (Luminal type), BT474 (HER2-enriched type), BT20 (Basal A type) or MM436 (Basal B type) with control or MICAL3 siRNA (pool siRNA). (B) SCM (EGF/bFGF/B27) or HRG-induced tumor sphere formation of human breast cancer cells was reduced by *MICAL3* knock-down.

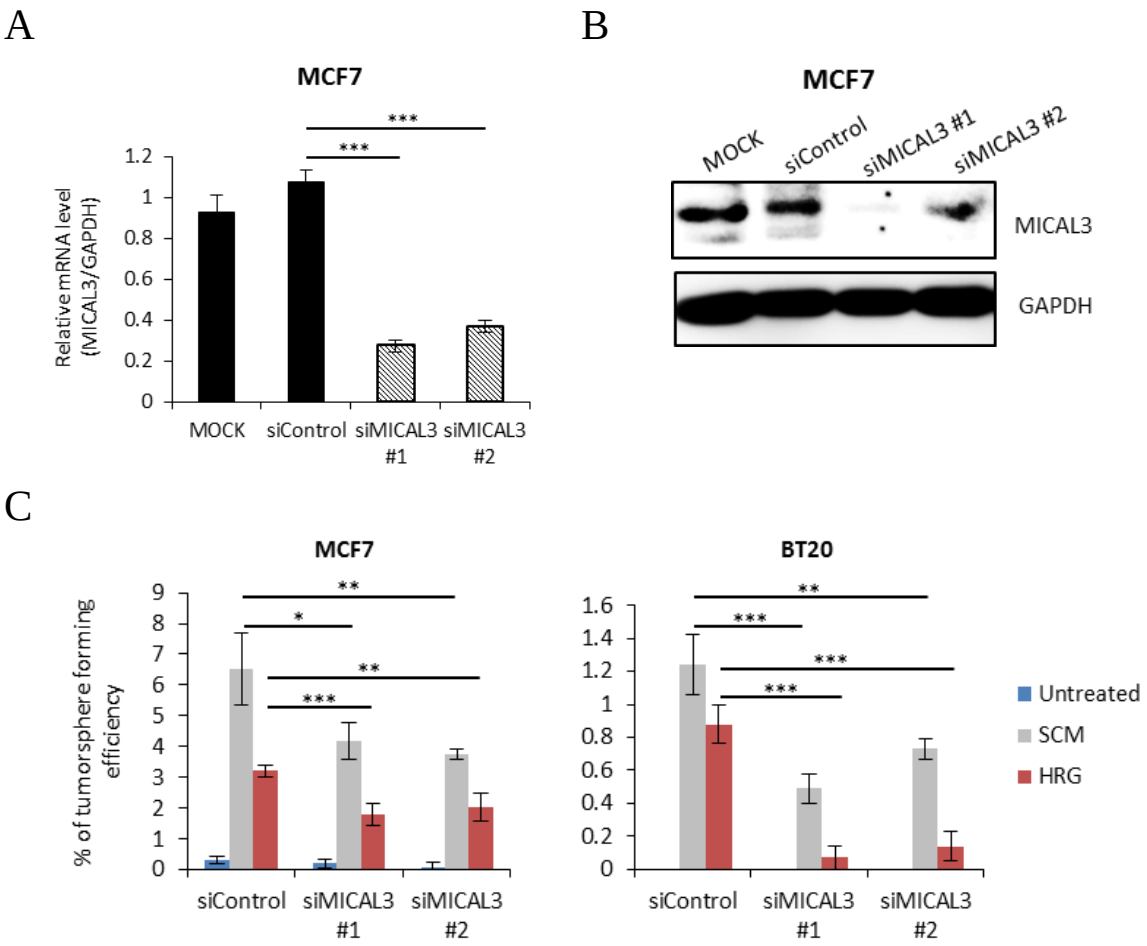

Figure 12

MICAL3 is a key factor for tumor sphere formation of human breast cancer cell lines.

(A) Expression of *MICAL3* mRNA by qRT-PCR in MCF7 cells with control or MICAL3 siRNA (individual siRNA). (B) Expression of MICAL3 protein by Immunoblotting in MCF7 cells with control or MICAL3 siRNA (individual siRNA). (C) SCM (EGF/bFGF/B27) or HRG-induced tumor sphere formation of MCF7 cells (Luminal type) or BT20 cells (Luminal type) was reduced by *MICAL3* knock-down.

A

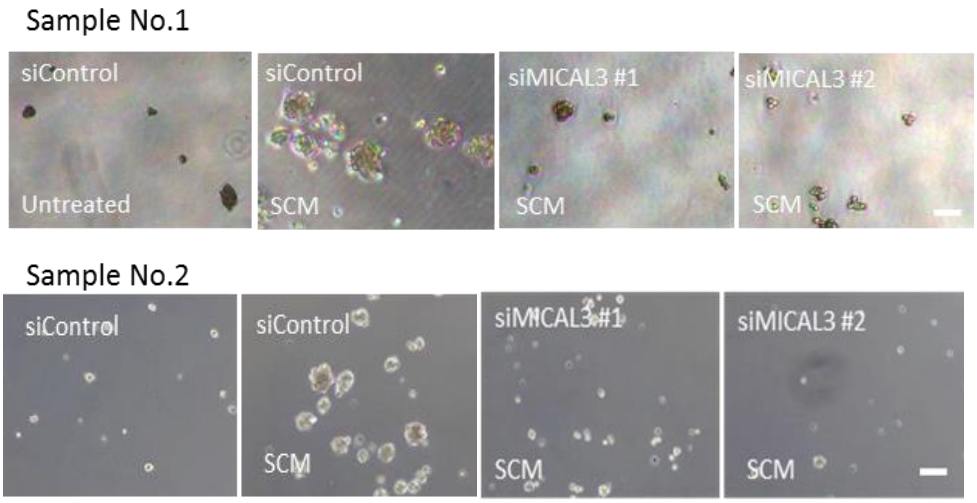

B

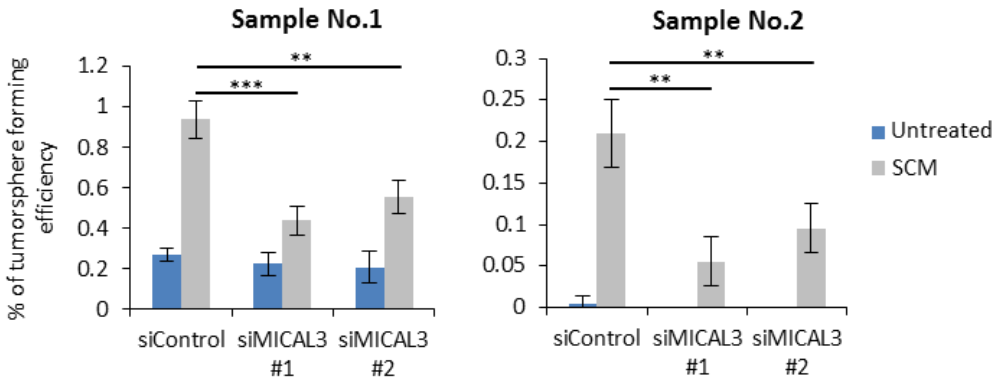

Figure 13

MICAL3 is a key factor for tumor sphere formation of patient-derived primary breast cancer cells.

(A) Representative phase contrast images of formed tumor spheres of patient-derived primary breast cancer cells using MICAL3 siRNA. Scale bar: 100 μm. (B) SCM-induced tumor sphere formation of patient-derived primary breast cancer cells was reduced by *MICAL3* knock-down.

A

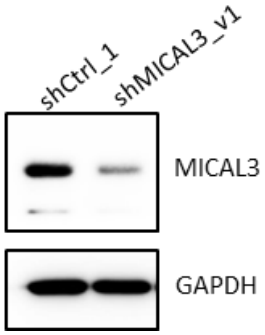

B

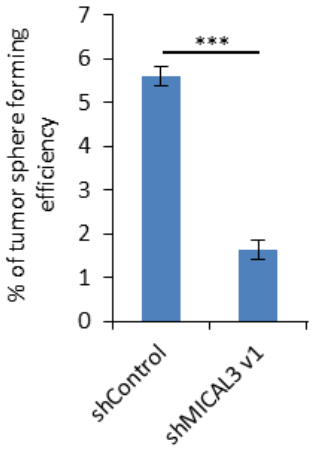

C

	Cells per site		Tumor initiating cell frequency estimate	P. value vs shControl
	10^3	10^4		
shControl	2/5	3/5	1/7115	
shMICAL3 v1	0/5	1/5	1/49,833	0.0383

D

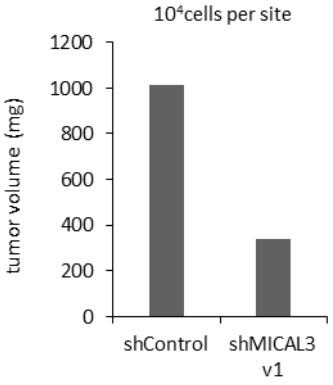

Figure 14

Knock-down of *MICAL3 variant 1 (v1)* decreases sphere forming ability and tumor initiating activity in MCF7 cells.

(A) Expression of MICAL3 protein by immunoblotting in MCF7 cells transduced with control or *MICAL3 v1* shRNA. (B) SCM (EGF/bFGF/B27)-induced tumor sphere formation of MCF7 cells was reduced by *MICAL3* knock-down. (C) 10^4 or 10^3 cells of MCF7 cells transduced with shControl, shRNA for *MICAL3 v1* were subcutaneously injected into the mammary fat pads of the eight-week-old female NSG mice. Results were obtained after 30 days after implantation. Frequency determinations were generated using ELDA software. (D) Tumor weight was measured at 30 days after implantation of MCF7 cells transduced with shControl or shRNA for *MICAL3 v1*.

A

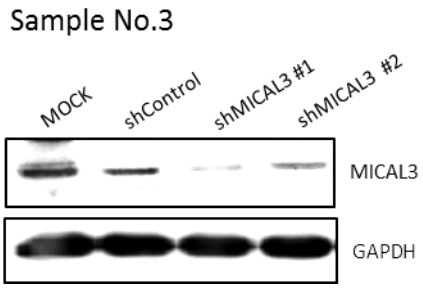

B

Sample No.3

	Cells per site			Tumor initiating cell frequency estimate	P. value vs shControl
	10	10^2	10^3		
shControl	4/6	6/6	6/6	1/10	
shMICAL3 #1	0/6	2/6	5/6	1/460	2.01e-08
shMICAL3 #2	1/6	5/6	6/6	1/56	0.0122

C

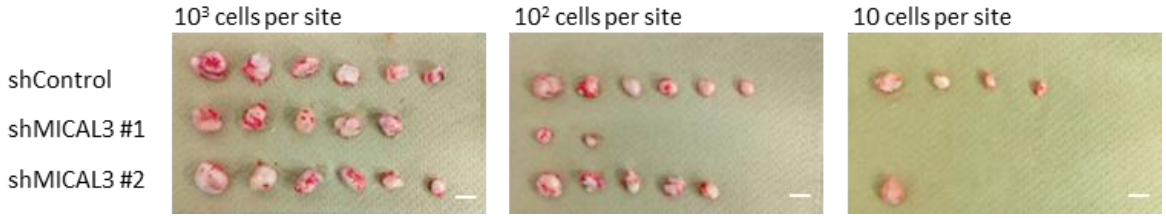

Figure 15

Knock-down of *MICAL3 v1* decreases sphere forming ability and tumor initiating activity in patient-derived breast cancer cells.

(A) Expression of MICAL3 protein by immunoblotting in MCF7 cells transduced with control or *MICAL3* shRNA. (B) 10^3, 10^2 or 10 cells of patient-derived breast cancer cells were subcutaneously injected into the mammary fat pads of the eight-week-old female NSG mice. Results were obtained after 60 days after implantation. Frequency determinations were generated using ELDA software. (C) Representative images of tumors generated in mice injected with cells described in (B). Scale bar: 1 cm.

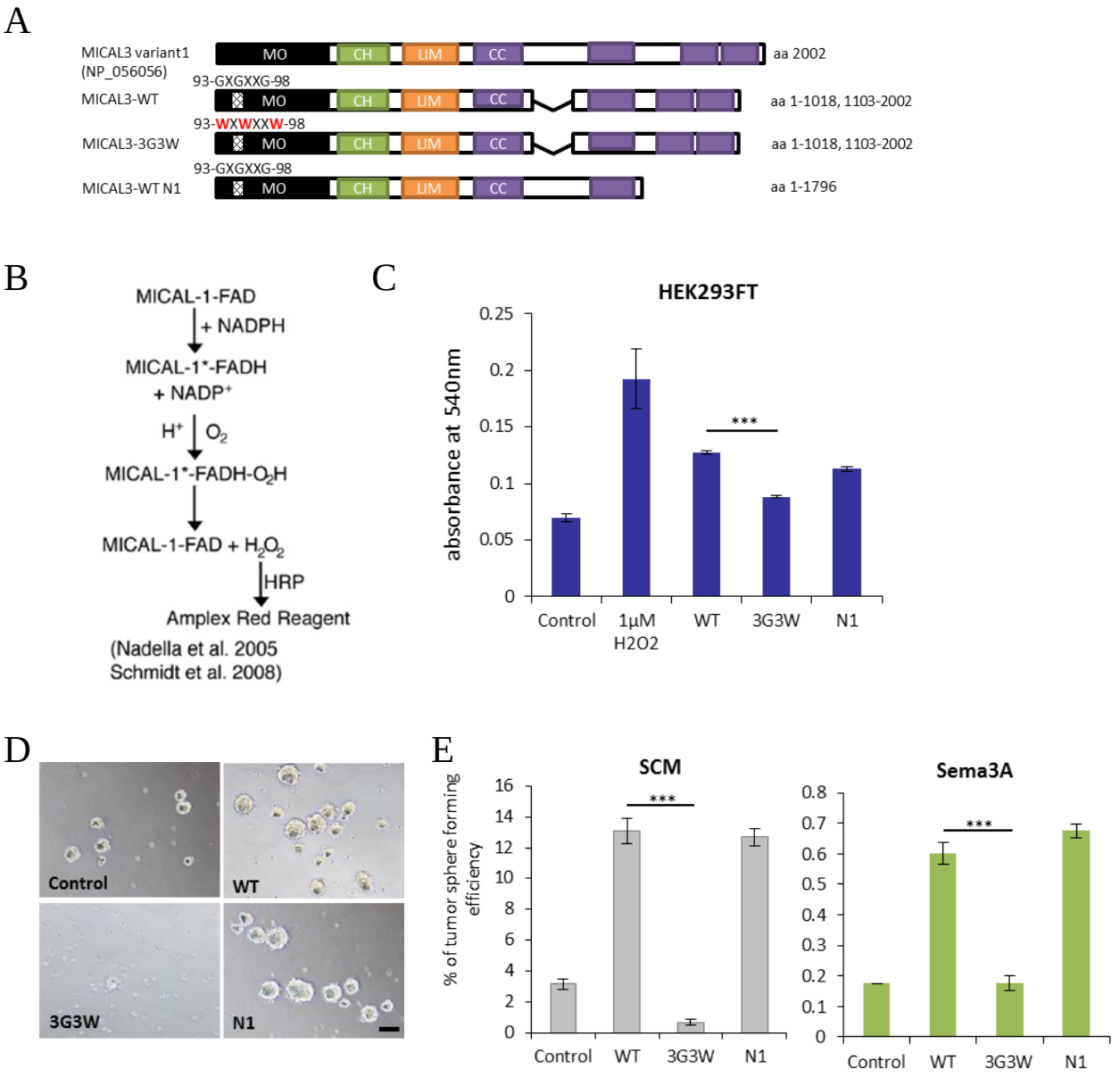

Figure 16

Monooxygenase domain of MICAL3 plays important role for tumor sphere formation.

(A) A schema of MICAL3 wild-type (WT) and mutants (3G3W and N1) constructs; MO, monooxygenase domain; CH, calponin homology domain; LIM, Lin11, Isl-1, Mec-3 domain (zinc binding); CC, coiled-coil domain. (B) Overview of the enzyme-linked assay used to determine H_2O_2 levels. (C) Measurement of H_2O_2 production using lysates of HEK293T cells transfected with the indicated constructs described in (A) in the presence of 200 µM NADPH. (D) Representative phase contrast images of formed tumor spheres of MCF7 cells transfected with the indicated constructs induced by SCM. Scale bar: 100 µm. (E) Tumor sphere formation of MCF7 cells transfected with the indicated constructs induced by SCM or Sema3A.

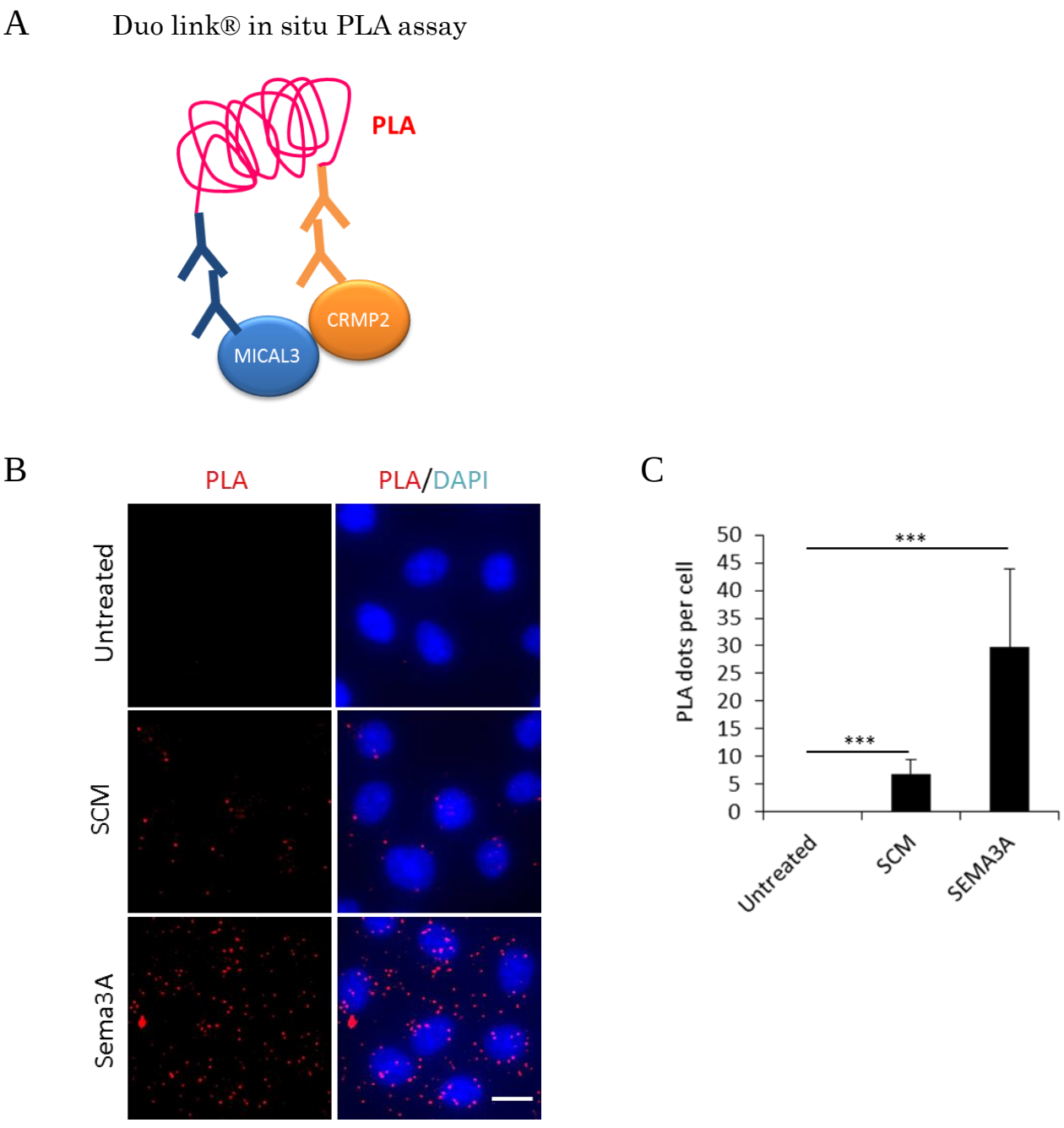

Figure 17

Interaction between MICAL3 and CRMP2.

(A) A schema of Duolink® in situ Proximity Ligation Assay (PLA). (B) In situ PLA shows the interaction between MICAL3 and CRMP2 in MCF7 cells as shown by red dots (arrows). Nucleus was stained by DAPI. Scale bar: 40 μm. (C) Quantification of the number of PLA dots per cells. Scale bar: 40 μm. 100 cells are counted and results showed by mean ± SD.

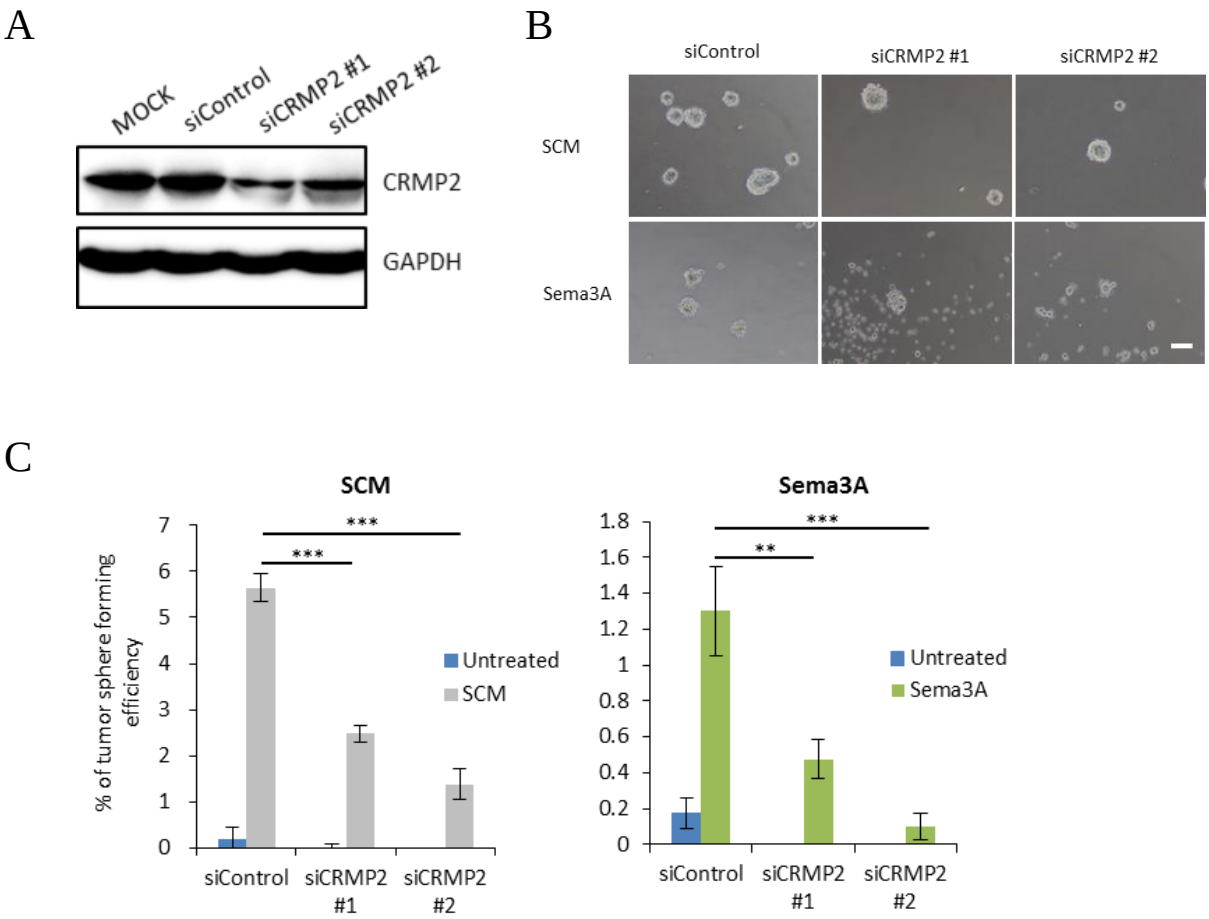

Figure 18

CRMP2 is a key factor for tumor sphere formation.

(A) Expression of CRMP2 protein by immunoblotting in MCF7 transfected with control or *CRMAP2* siRNA. (B) Representative phase contrast images of formed tumor spheres of MCF7 cells transfected with *CRMP2* siRNA induced by SCM (upper panels) or Sema3A (lower panels). Scale bar: 100 μm. (C) Tumor sphere formation of MCF7 cells transfected with *CRMP2* siRNA induced by SCM (left panel) or Sema3A (right panel).

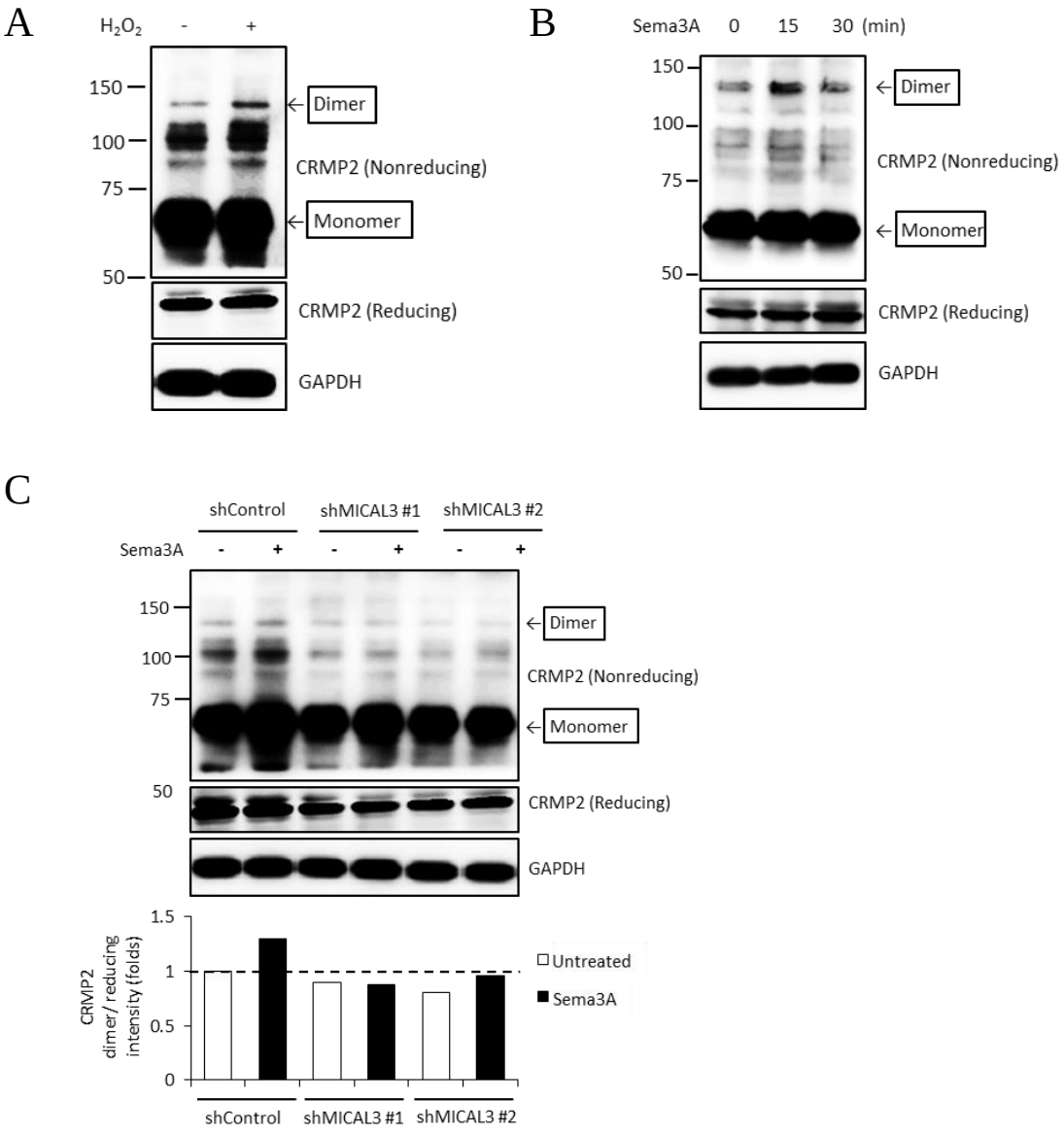

Figure 19

Sema3A-induced dimer formation of CRMP2 is inhibited by *MICAL3* knock-down.

(A) Immunoblotting analysis of the expression of CRMP2 protein in MCF7 cells following stimulation with or without 1μM H_2O_2. Cell lysates were immunoblotted with anti-CRMP2 antibodies under nonreducing conditions. Reducing condition was assayed as a positive control. GAPDH was blotted as a loading control. (B) Immunoblotting analysis of the expression of CRMP2 protein in MCF7 cells following stimulation with or without 200ng/ml Sema3A. (C) Immunoblotting analysis of the expression of CRMP2 protein in MCF7 cells transduced with control or *MICAL3* shRNA by stimulation with or without 200ng/ml Sema3A.

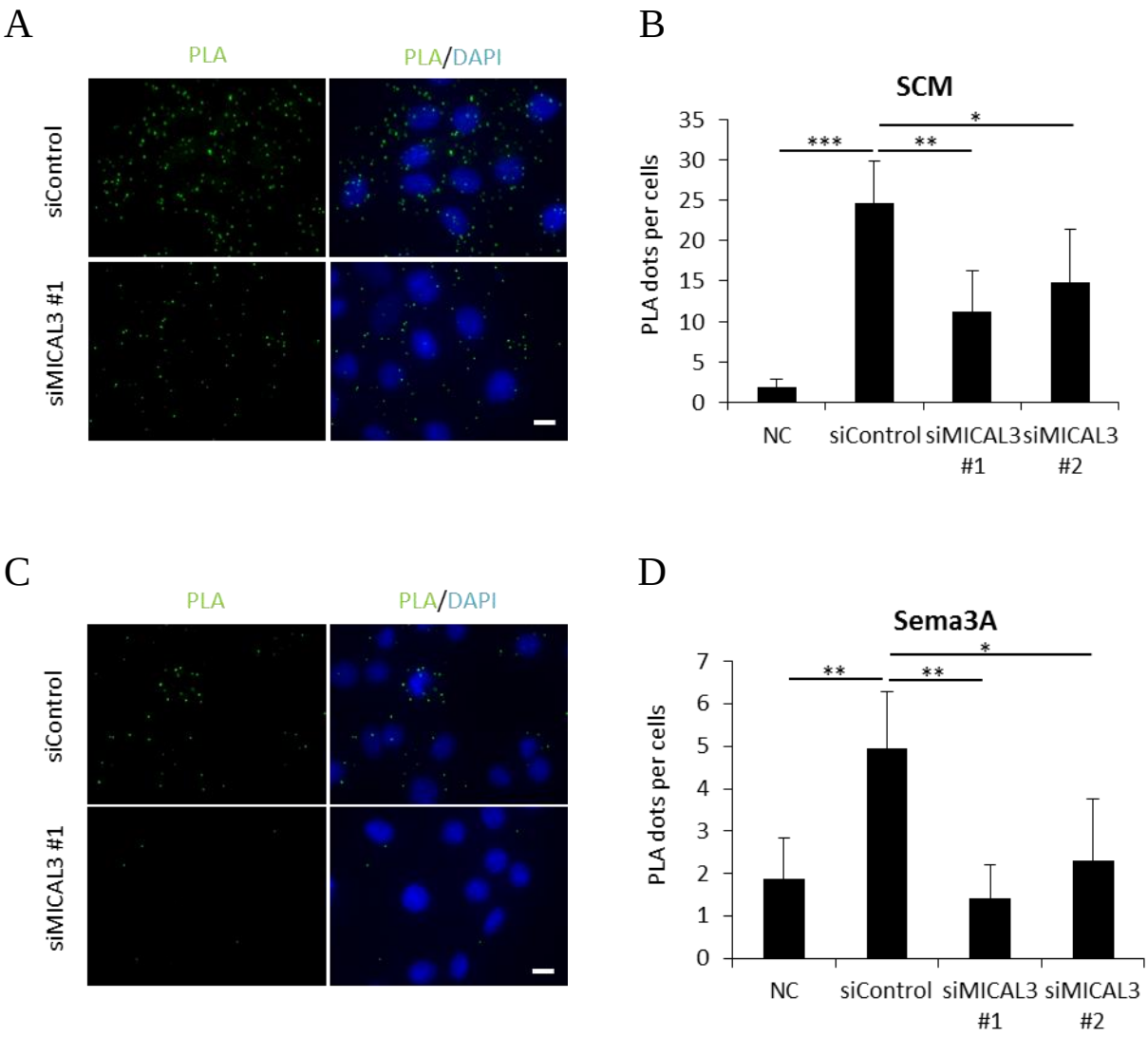

Figure 20

MICAL3 is required for the interaction between CRMP2 and NUMB in MCF7 cell induced by SCM or Sema3A.

(A) In situ PLA showed interaction between CRMP2 and NUMB by SCM treatment for 24 hours and it was reduced by knock-down of *MICAL3* in MCF7 cells. PLA dots (green) indicate the interaction between CRMP2 and NUMB. Scale bar: 40 μm (B) Quantification of the number of PLA dots per cells shown in (A). 20 cells are counted and results showed by mean ± SD. (C) In situ PLA showed interaction between CRMP2 and NUMB by Sema3A stimulation for 24 hours and it was reduced by knock-down of *MICAL3* in MCF7 cells. PLA dots (green) indicate the interaction between CRMP2 and NUMB. Scale bar: 40 μm (D) Quantification of the number of PLA dots per cells shown in (C). 20 cells are counted and results showed by mean ± SD.

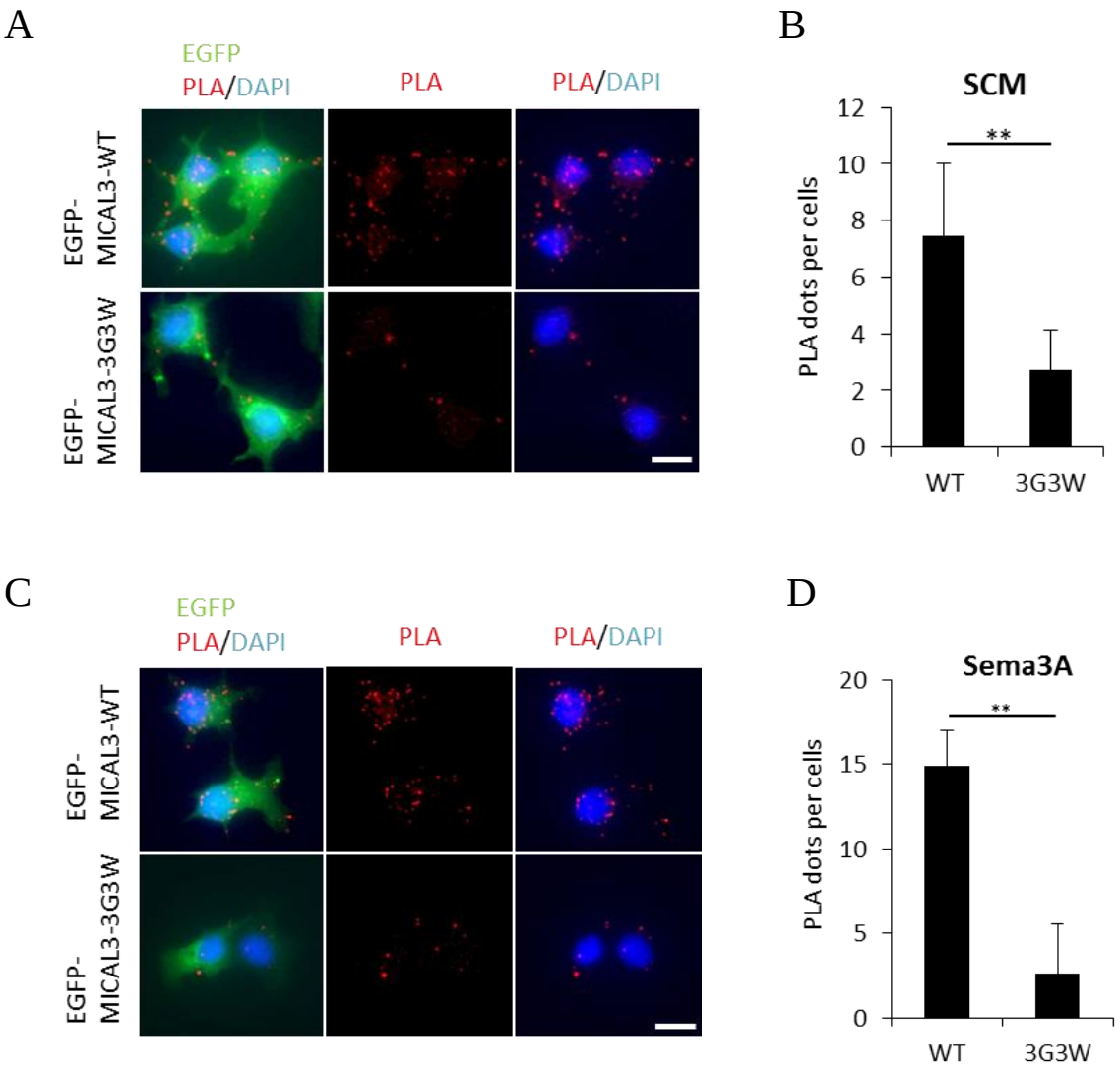

Figure 21

Monooxygenase domain of MICAL3 is required for the interaction between CRMP2 and Numb in MCF7 induced by SCM or Sema3A.

(A) In situ PLA showed interaction between CRMP2 and NUMB by SCM treatment for 24 hours in MCF7 cells transfected with MICAL3-WT or 3G3W cDNA construct. PLA dots (red) indicate the interaction between CRMP2 and Numb. Scale bar: 40 μm (B) Quantification of the number of PLA dots per cells shown in (A). 20 cells are counted and results showed by mean ± SD. (C) In situ PLA showed interaction between CRMP2 and Numb by Sema3A stimulation for 24 hours in MCF7 cells transfected with MICAL3-WT or 3G3W cDNA construct. Scale bar: 40 μm (D) Quantification of the number of PLA dots per cells shown in (C). 20 cells are counted and results showed by mean ± SD.

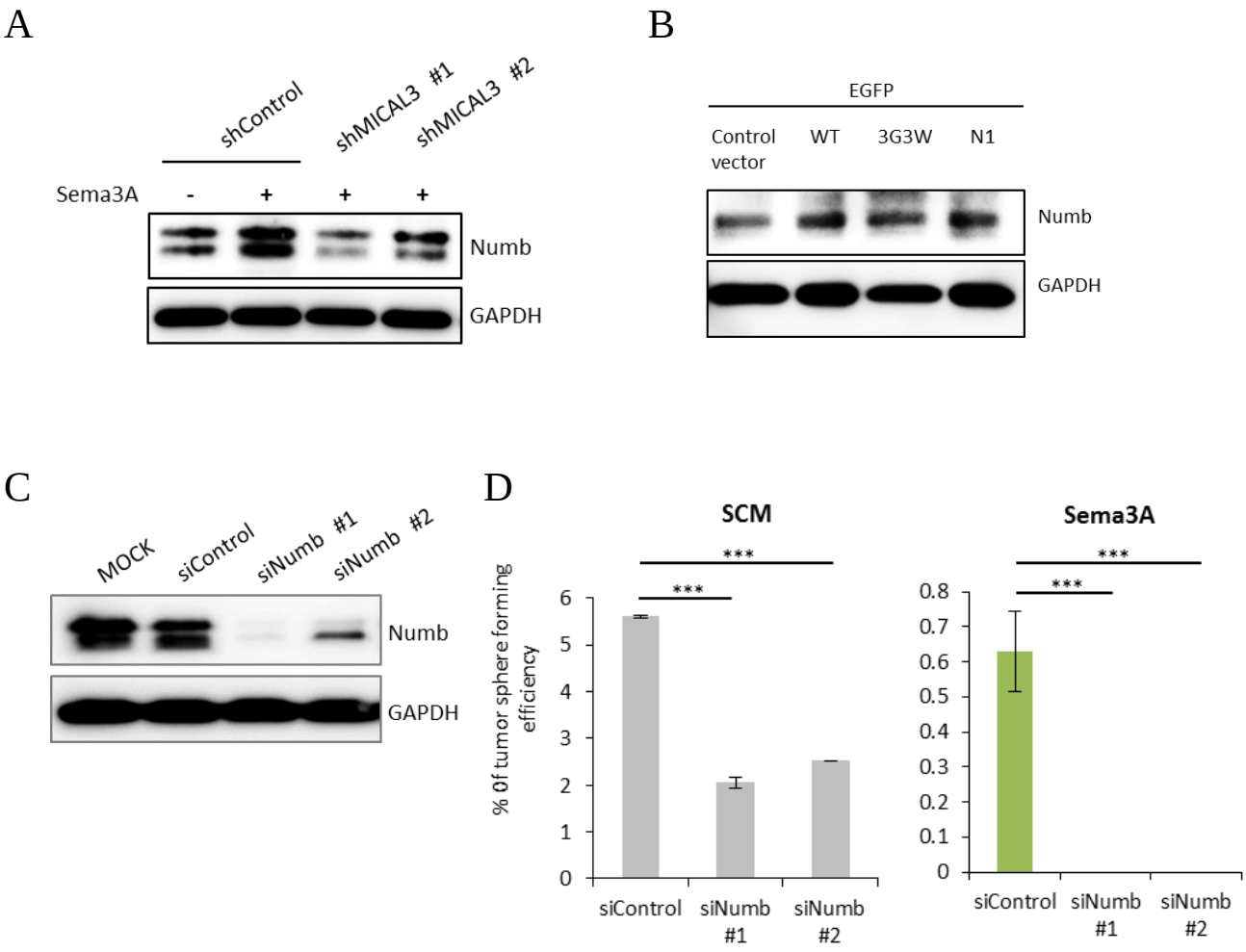

Figure 22

Sema3A induces expression of Numb protein and knock-down of *Numb* reduces tumor sphere formation

(A) Immunoblotting analysis of expression of Numb protein in MCF7 cells transfected with control or *MICAL3* siRNA by stimulation with or without Sema3A. (B) Immunoblotting analysis of Numb protein in MCF7 cell transfected with the indicated constructs. (C) Immunoblotting analysis of Numb protein in MCF7 cells transfected with control or *Numb* siRNA. (D) Tumor sphere formation of MCF7 cells transfected with *Numb* siRNA induced by SCM (left panel) or Sema3A (right panel).

A

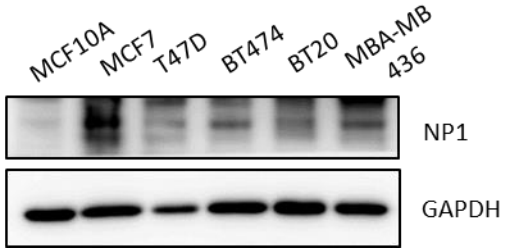

B

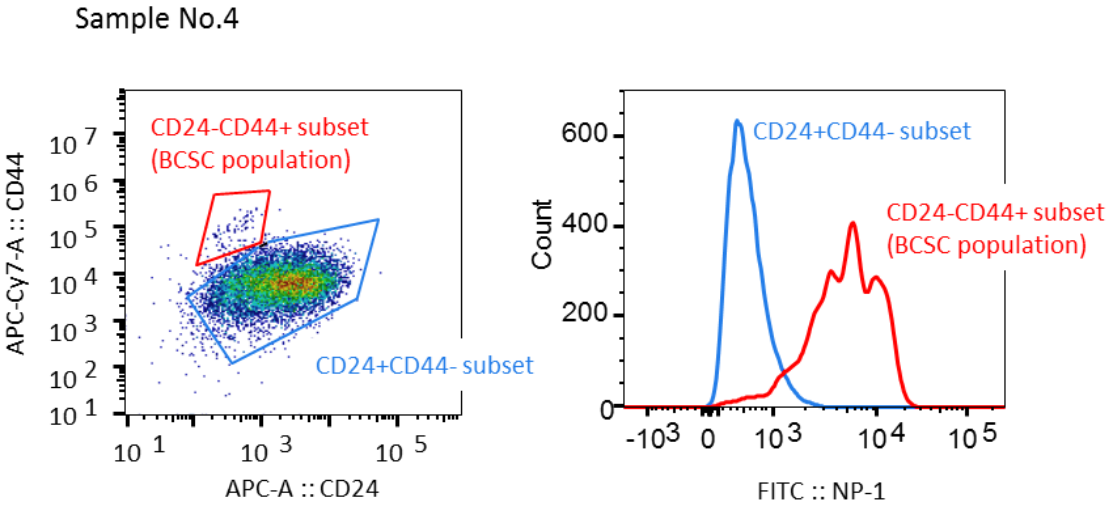

Figure 23

NP1 is predominantly expressed in BCSC-enriched population

(A) Expression of NP1 protein by immunoblotting in several human breast cancer cell lines and non-cancerous MCF10A cells.

(B) FACS analysis of freshly obtained patient-derived breast cancer cells (Sample No.4). The cells were sorted according to the expression of CD44 and CD24. The $CD44^{high}/CD24^{low}$ BCSC-enriched population and the other population were then sorted according to the expression of NP1.

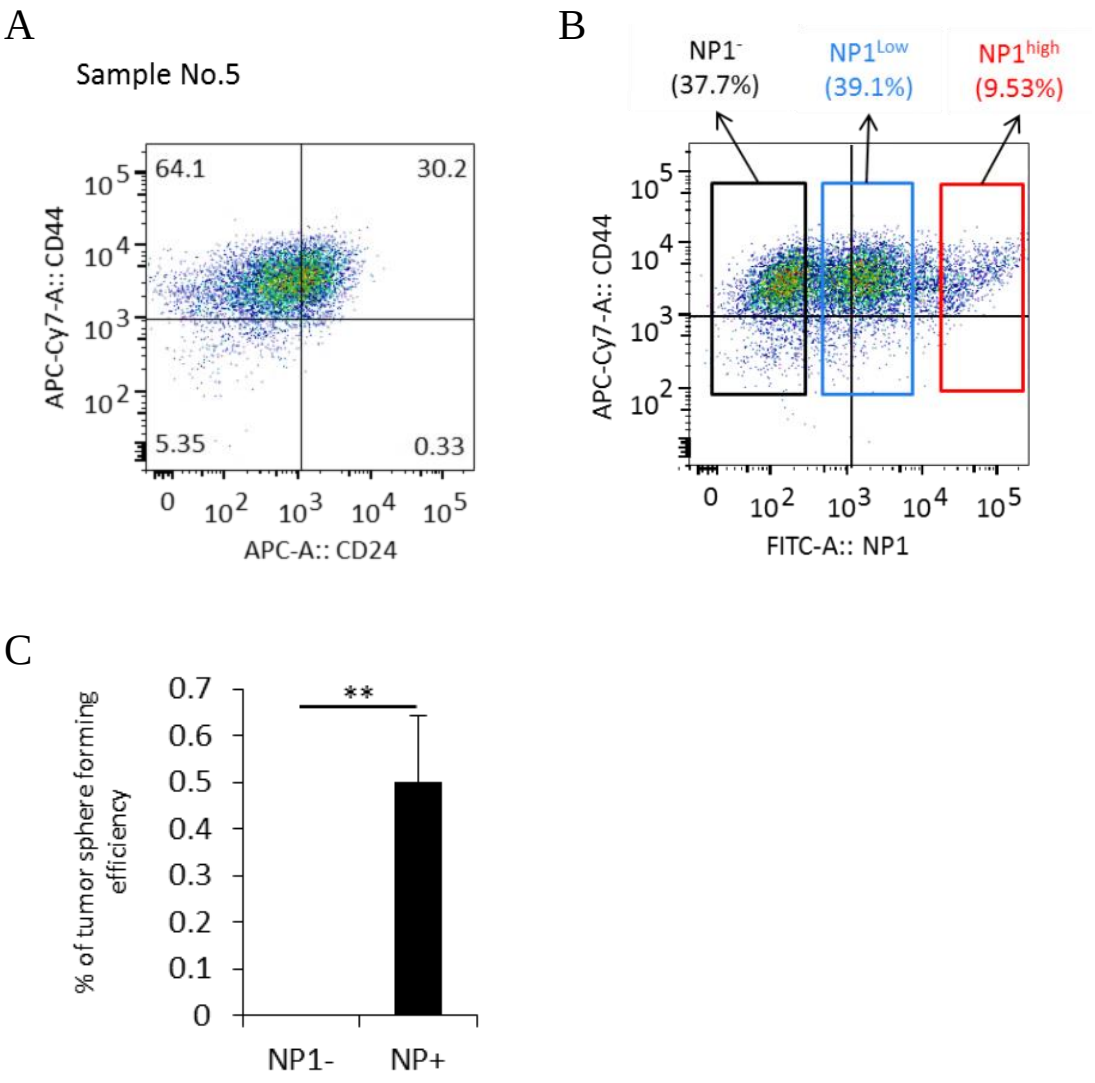

Figure 24

NP1-highly positive cell population shows strong sphere forming activity

(A) FACS analysis of freshly obtained patient-derived breast cancer cells (Sample No.5). The cells were sorted according to the expression of CD44 and NP1. (B) NP1-highly positive cells but not NP1-negative cells of patient-derived breast cancer cells induced tumor sphere formation in SCM.

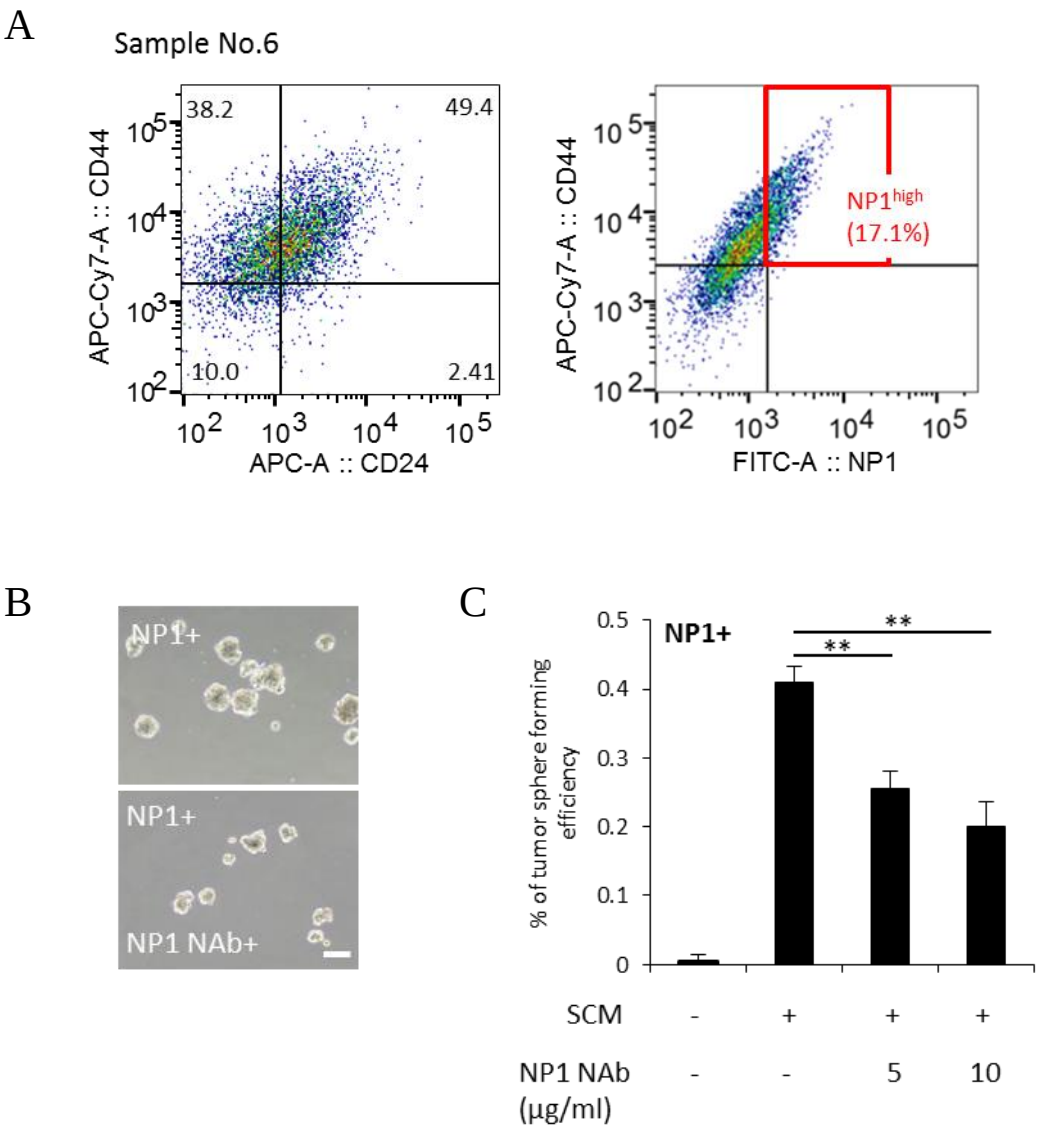

Figure 25

NP1-highly positive cell population shows strong sphere forming activity

(A) FACS analysis of freshly obtained patient-derived breast cancer cells (Sample No.6). The cells were sorted according to the expression of NP1. (B) Representative phase contrast images of sphere formation by patient-derived breast cancer cells with highly positive NP1 in the presence or absence of an anti-NP1 neutralizing antibody (NP1 NAb) in SCM. Scale bar: 100 μm. (D) Quantification of the sphere forming activity of the cells with highly positive in SCM. Sphere forming ability of NP1 highly positive cells was significantly reduced by treatment with an NP1 NAb.

A

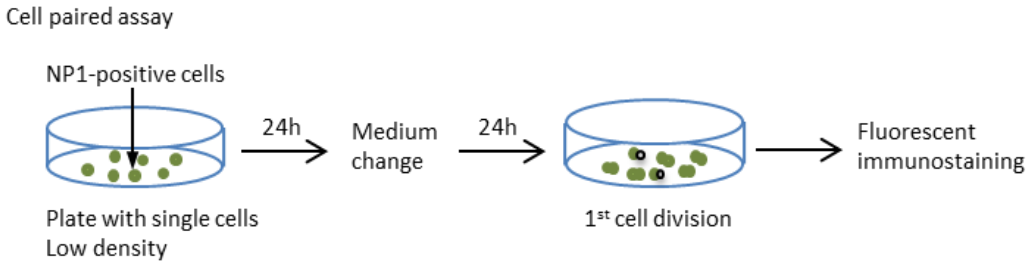

B

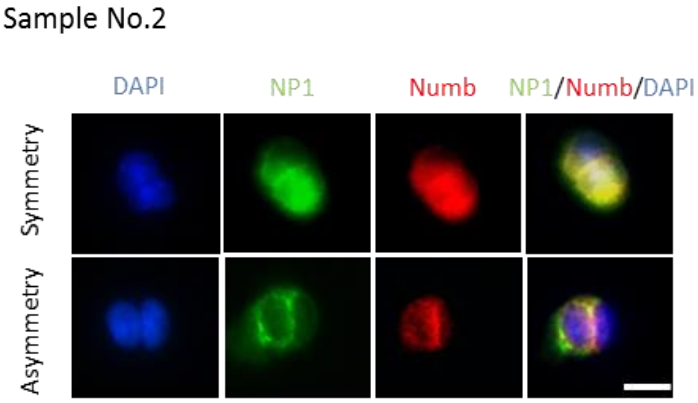

C

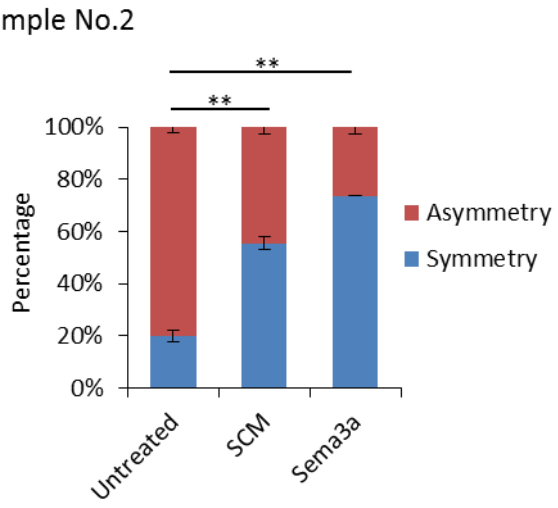

Figure 26

NP1 and Numb co-localize in patient-derived breast cancer cells and SCM increases symmetric cell division

(A) A schema of cell paired assay using patient-derived breast cancer cells.

(B) Immunofluorescence for Numb and NP1 in cell-paired assays showed co-localization of the two proteins in patient-derived breast cancer cells. The nucleus was stained by DAPI. Scale bar: 40 μm (C) Quantificaiton of the percentage of symmetric/asymmetric division. 20 cells are counted and results showed by mean ± SD.

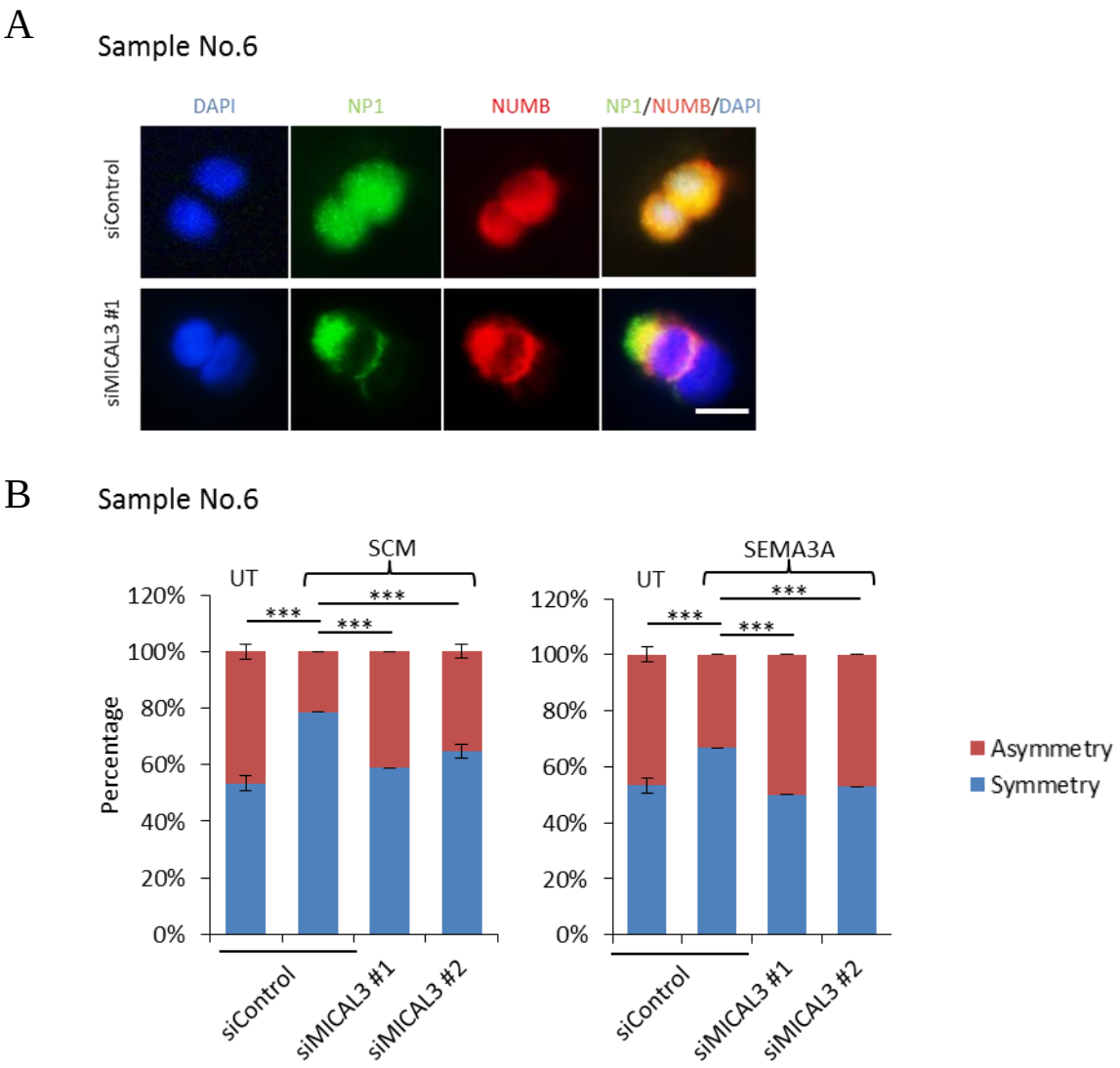

Figure 27

SCM or Sema3A-increased symmetric cell division is reduced by knock-down of *MICAL3*

(A) Immunofluorescence for Numb and NP1 in cell-paired assays showed symmetric/asymmetric cell division. Symmetric cell division was reduced by *MICAL3* knockdown using siRNA. The nucleus was stained by DAPI. Scale bar: 40 μm

(B) Quantification of the percentage of asymmetric or symmetric division of NP1 positive cells. UT means untreated cells. 10 cells are counted and results showed by mean ± SD.

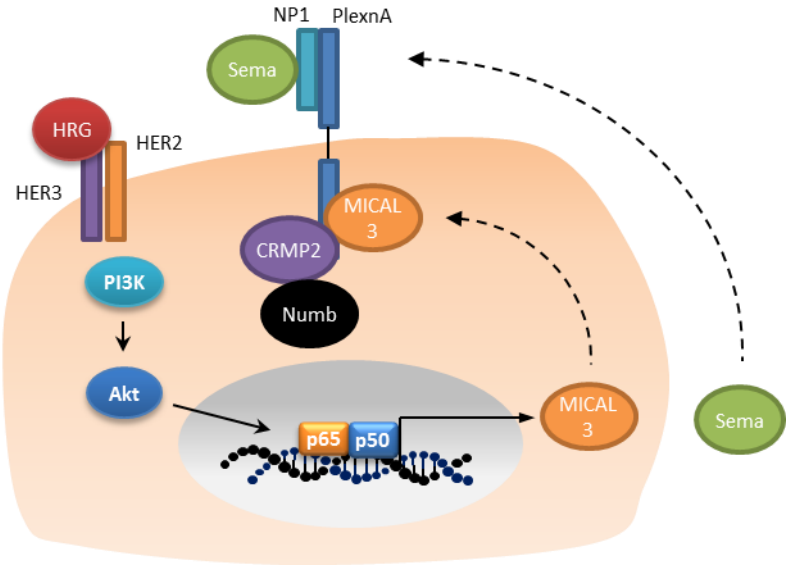

Figure 28

Semaphorin/MICAL3/CRMP2 axis increases symmetric division of NP1-positive cancer stem-like cells in human breast cancer

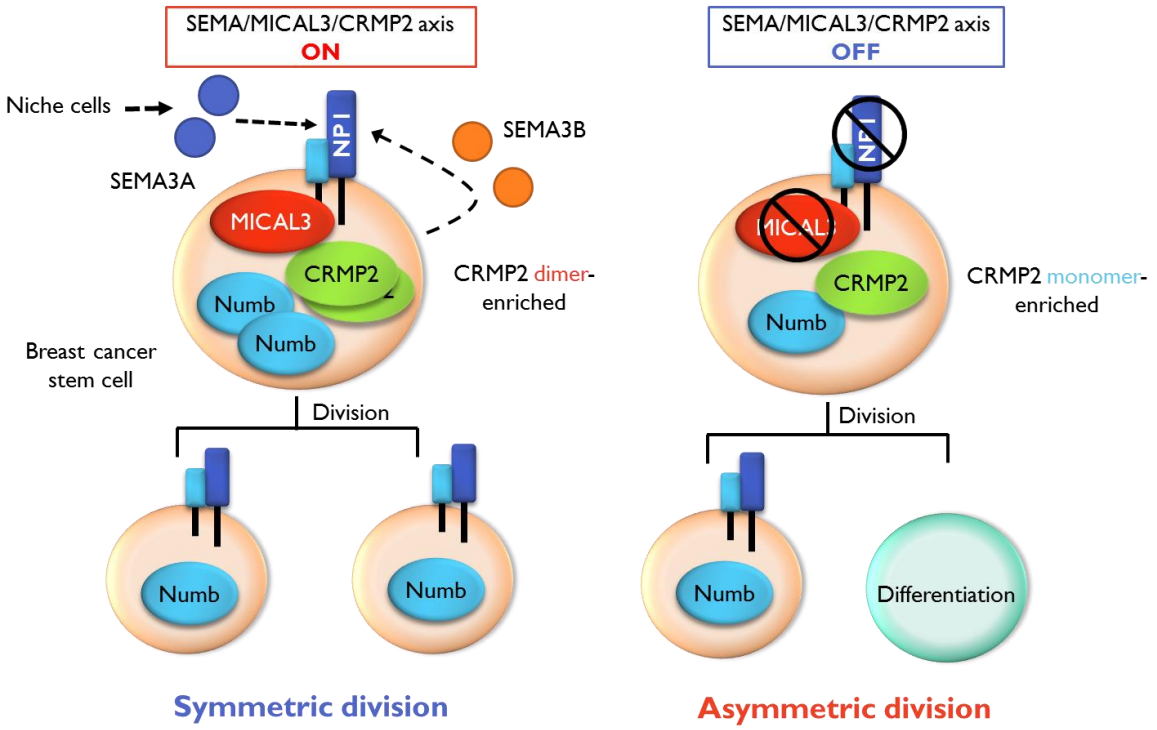

Figure 29

Semaphorin/MICAL3/CRMP2 axis increases symmetric division of NP1-positive cancer stem-like cells in human breast cancer

siRNA (ON-TARGETplus)	Target Sequence
MICAL3 #1	5′-CCAAGAGAAUGAACGGAUA-3′
MICAL3 #2	5′-CCGUACAGCCAUCGACUUA-3′

Table 1

The target sequences of MICAL3 siRNAs (ON-TARGETplus).

shRNA	Sequence
Control	5′-GATCCCCGTGTGCTTTGTAGGGTTCTACGTGTGCTGTCCGTAGAATCCTACAAAGCGCGCTTTTTGGAAAT-3′ 5′-CTAGATTTCCAAAAAGCGCGCTTTGTAGGATTCGACGGACAGCACACGTAGAACCCTACAAAGCACACGGG-3′
MICAL3 variant 1 #1	5′-GATCCCCGATGTGCGCTGGACTCGTATAACGTGTGCTGTCCGTTATATGAGTCCAGTGCACGTCTTTTTGGAAAT-3′ 5′-CTAGATTTCCAAAAAGACGTGCACTGGACTCATATCACGGACAGCACACGTTATACGAGTCCAGCGCACATCGGG-3′
MICAL3 variant 1 #2	5′-GATCCCCGGGAGTTCCTCCGACATGGAAACGTGTGCTGTCCGTTTTCATGTTGGAGGAGCTCCCTTTTTGGAAAT-3′ 5′-CTAGATTTCCAAAAAGGGAGCTCCTCCAACATGAAGACGGACAGCACACGTTTCCATGTCGGAGGAACTCCCGGG-3′

Table 2

The sequences of MICAL3 shRNA plasmids.

siRNA (StealthTM RNAi)	Sequence
SEMA3B #1	5′-GACGGACACUAUGACGUCCUCUUCA-3′ 5′-UGAAGAGGACGUCAUAGUGUCCGUC-3
NUMB #1	5′-GACCGAUGGUUAGAAGAGGUGUCUA-3′ 5′-UAGACACCUCUUCUAACCAUCGGUC-3′
NUMB #2	5′-GAGAAAGAAGGAUGUUUAUGUUCCA-3′ 5′-UGGAACAUAAACAUCCUUCUUUCUC-3′
CRMP2 #1	5′-GGGUAAAUUCCUUCCUCGUGUACAU-3′ 5′-AUGUACACGAGGAAGGAAUUUACCC-3′
CRMP2 #2	5′-GCUCUUCAAAGAUCGCUUCCAGCUAA-3′ 5′-UUAGCUGGAAGCGAUCUUUGAAAGC-3′

Table 3

The sequences of siRNAs (Stealth^{TM} RNAi) .